AIMS Mathematics, 11(6): 16199–16234.
DOI: 10.3934/math.2026666
Received: 03 March 2026
Revised: 19 May 2026
Accepted: 20 May 2026
Published: 08 June 2026

https://www.aimspress.com/journal/Math

Research article

Event-triggered sliding mode control for differential-drive mobile robots

Zhiqiang Chen[1], **Duzhesheng Liao**[1,2*] **and Wanghui Yang**[3]

[1] Faculty of Control Systems and Robotics, ITMO University, Kronverkskiy ave 49, St. Petersburg, Leningrad Region, Russia

[2] School of Information Science and Technology, Zhejiang Shuren University, Hangzhou 310015, China

[3] School of Management, Hangzhou Dianzi University, Hangzhou 310018, China

* **Correspondence:** Email: ldzs2015@gmail.com.

Abstract: In this paper, we investigated trajectory tracking control for differential-drive mobile robots under unknown disturbances and limited communication resources. To address the singularity problem and the trade-off between high-precision finite-time tracking and communication resource conservation, we proposed a novel event-triggered sliding mode control scheme. The scheme achieved three major results: First, a specially designed sliding surface eliminated the singularity problem and ensured high convergence accuracy. Second, an adaptive disturbance observer accurately estimated unknown disturbances without requiring prior information. Third, an event-triggered mechanism significantly reduced communication demands while maintaining control performance. Importantly, the proposed controller avoided the high-gain issues present in methods. Comparative MATLAB simulations demonstrated faster convergence, smaller steady-state errors, and a favorable balance between tracking precision and communication efficiency.

Keywords: differential-drive mobile robot; finite time stability; sliding mode control; event-triggered control; disturbance observer
Mathematics Subject Classification: 93C10

1. Introduction

Differential-drive mobile robots (DDMRs) are widely used in industrial automation, service robotics, and autonomous exploration due to their simple structure and high maneuverability [1–3]. However, achieving high-precision trajectory tracking for DDMRs remains a challenging task. This difficulty stems from their inherent nonholonomic constraints and the presence of unknown disturbances in practical operating environments. Currently, significant advancements have been

made in control methodologies. For example, nonlinear state feedback [4, 5] is widely used for underactuated system regulation. Model predictive control [6, 7] handles constraints via receding horizon optimization. Disturbance observer-based robust control [8, 9] effectively compensates for external disturbances and model uncertainties. However, none of the above methods fully resolve the three-way trade-off among convergence speed, steady-state precision, and computational efficiency.

Sliding mode control (SMC) has emerged as an attractive approach for trajectory tracking of DDMRs owing to its inherent robustness against matched uncertainties and ease of implementation [10]. Within the SMC framework, terminal sliding mode control (TSMC) offers finite-time convergence of system states via nonlinear sliding surfaces, making it particularly suitable for high-precision tracking control of DDMRs [11–13]. However, The application of TSMC to DDMRs faces two fundamental issues: the singularity problem and the convergence accuracy problem.

The singularity problem arises from the negative fractional powers in the derivative of conventional TSMC surfaces. Consider a typical TSMC surface $s = \dot{e} + \beta e^{p/q}$, where $0 < p/q < 1$. Its derivative contains the term $e^{p/q-1}$, which tends to infinity as $e \to 0$, causing divergence of the control input. To mitigate this issue, researchers have developed non-singular terminal sliding mode control (NTSMC). One common approach is to swap the positions of the error and its derivative in the surface design [12, 13]. Another method involves introducing piecewise functions that switch to a linear region near the origin [14, 15]. However, when applying these NTSMC designs to DDMR platforms, a new issue emerges: The convergence time of the robot states depends on the instantaneous pose error. For instance, the adaptive fast NTSMC proposed in [16] successfully eliminates singularity, yet its convergence time upper bound explicitly depends on the instantaneous tracking error. This implies that the upper bound of the convergence time cannot be determined a priori.

Parallel to the development of SMC, disturbance observer techniques have been widely integrated into the control framework of DDMRs to enhance robustness by estimating and compensating unknown disturbances in real time [17, 18]. Specifically, the researchers in [17] designed a disturbance observer-based control scheme for manipulators with unknown actuator faults to improve their robustness. For the problem of unmanned aerial vehicle formation control with unknown actuator faults and input saturation, the researchers in [18] designed a sliding mode disturbance observer to estimate unknown disturbances and actuator faults online. Subsequently, researchers further proposed finite-time/fixed-time disturbance observers to address the convergence speed issue. The researchers in [19] designed a fixed-time disturbance observer for quadrotor UAVs to mitigate the impact of environmental disturbances. To mitigate the effect of tire slippage on mobile robots, the researchers in [20] analyzed the kinematic model of mobile robots under tire slipping and proposed a fixed-time control scheme based on a sliding mode observer. However, the sign function required to achieve finite-time convergence induces chattering, which accelerates actuator wear of DDMRs and reduces the service life of motors [21]. To suppress chattering, existing methods (e.g., [22, 23]) employ continuous saturation functions or sigmoid functions to replace the discontinuous sign function when designing formation controllers for mobile robots. The resulting controllers and observers are free from chattering. Nevertheless, this approximate smoothing inevitably impairs the robot's trajectory tracking accuracy. Thus, most methods cannot simultaneously achieve high accuracy and smoothness. Furthermore, although finite-time controllers for DDMRs guarantee that the system enters a residual set within finite time, the size of this residual set, namely, the steady-state

error, is often overlooked in theoretical analyses [24–26]. For example, the sliding mode controller in [26] can confine the trajectory tracking error of a mobile robot within an adjustable boundary, but it does not provide an explicit bound for that boundary. In [27], the researchers designed a super-twisting sliding mode controller that ensures finite-time convergence of the robot, with its steady-state accuracy determined by unknown residual terms and controller gains. However, these gains must be chosen conservatively to cope with worst-case disturbances. When the robot requires high-precision trajectory tracking, these methods cannot meet the requirements through simple parameter tuning. Therefore, the high-precision control problem for DDMRs remains challenging.

These challenges become even more severe in practical deployment. Event-triggered control provides an elegant solution by updating control signals only when preset conditions are violated [28, 29]. For cooperative robot object manipulation, the researchers in [28] proposed a simple yet effective event-triggered coordination strategy that significantly reduces communication and state update frequencies. The researchers in [29] combined the high-order fully actuated system approach with an event-triggered mechanism to develop a dynamic event-triggered controller based on a matrix threshold strategy for single-link flexible joint robot systems. Event-triggered sliding mode controllers have been proposed for robotic systems [30–32]. For DDMRs, the researchers in [31] proposed an event-based sliding mode controller that guarantees a minimum inter-event time, excludes Zeno behavior, and validates the effectiveness through physical experiments. Tran et al. [32] designed an adaptive event-triggered sliding mode controller for DDMRs considering the case where the input matrix is non-square. Nath et al. [33] investigated reference trajectory tracking control of nonholonomic wheeled mobile robots using event-triggered sliding mode control, employing dynamic feedback linearization for controller design. However, this method suffers from a critical structural flaw: The determinant of the input matrix becomes zero under specific error conditions, leading to singularity and consequently high-gain phenomena. This singularity-high-gain dilemma may result in finite-time escape of the sliding variables, fundamentally limiting the practical applicability of the method.

In summary, the major contributions of this paper are as follows:

(1) A novel scalar nonlinear function is proposed to construct a finite-time sliding surface. In contrast to other studies [25–27], the proposed sliding surface not only eliminates singularity issues but also guarantees that the tracking error converges to a predefined and adjustable region, thereby significantly improving convergence accuracy.

(2) In contrast to the disturbance observers presented in [20–22], the proposed observer achieves chattering-free estimation and exhibits higher estimation accuracy without requiring prior knowledge of disturbance bounds.

(3) The event-triggered sliding mode control scheme proposed in this paper eliminates singular control inputs, thereby avoiding the high-gain control issues and finite-time escape phenomena present in [33].

The remainder of this paper is organized as follows. In Section 2, we present the problem formulation and preliminaries, including the piecewise nonlinear function and its key properties. In Section 3, we provide the major results; the co-design of the disturbance observer, finite-time controller, and event-triggering mechanism. In Section 4, we validate the theoretical analysis through comprehensive comparative simulations. In Section 5, we conclude the paper and discuss future research directions.

2. Problem formulation and preliminaries

The kinematic model of a differential-drive mobile robot is given by:

$$\dot{\mathbf{q}} = \mathbf{S}(\theta)\mathbf{V} = \begin{bmatrix} \cos\theta & 0 \\ \sin\theta & 0 \\ 0 & 1 \end{bmatrix} \begin{bmatrix} v \\ \omega \end{bmatrix}, \tag{2.1}$$

where $\mathbf{q} = [x, y, \theta]^{\mathrm{T}} \in \mathbb{R}^3$ denotes the posture vector, with (x, y) representing the Cartesian coordinates and θ the orientation angle. The control input $\mathbf{V} = [v, \omega]^{\mathrm{T}} \in \mathbb{R}^2$ comprises the linear and angular velocities.

For a given reference trajectory $\mathbf{q}_r(t) = [x_r(t), y_r(t), \theta_r(t)]^{\mathrm{T}} \in \mathbb{R}^3$, the posture tracking error expressed in the robot's body-fixed frame is defined as:

$$\mathbf{E} = \mathbf{R}(\theta)(\mathbf{q}_r - \mathbf{q}) = \begin{bmatrix} \cos\theta & \sin\theta & 0 \\ -\sin\theta & \cos\theta & 0 \\ 0 & 0 & 1 \end{bmatrix} \begin{bmatrix} x_r - x \\ y_r - y \\ \theta_r - \theta \end{bmatrix}, \tag{2.2}$$

where $\mathbf{R}(\theta)$ is the rotation matrix and $\mathbf{E} = (E_x, E_y, E_\theta)^{\mathrm{T}}$ is the posture tracking error vector.

The corresponding error dynamics are:

$$\dot{\mathbf{E}} = \begin{bmatrix} \omega E_y - v + v_r \cos E_\theta \\ -\omega E_x + v_r \sin E_\theta \\ \omega_r - \omega \end{bmatrix}, \tag{2.3}$$

where $v_r(t)$ and $\omega_r(t)$ denote the reference linear and angular velocities, respectively.

In practical applications, mobile robots are inevitably subject to external disturbances. The posture tracking error dynamics under matched disturbances can be described as [33]:

$$\begin{cases} \dot{E}_x = (\omega + d_2)E_y - (v + d_1) + v_r \cos E_\theta, \\ \dot{E}_y = -(\omega + d_2)E_x + v_r \sin E_\theta, \\ \dot{E}_\theta = \omega_r - (\omega + d_2), \end{cases} \tag{2.4}$$

where d_1 and d_2 represent external disturbances affecting the linear and angular velocity channels, respectively.

To address the chattering and singularity issues inherent in traditional finite-time sliding mode control, we introduce a nonlinear piecewise function $\Psi(x)$: $\mathbb{R} \to \mathbb{R}$ defined as:

$$\Psi(x) = \mathrm{sign}(x) f(x), \tag{2.5}$$

where the function $f(x)$: $\mathbb{R} \to \mathbb{R}^+$ is constructed in a piecewise manner:

$$f(x) = \begin{cases} f_1(x), & |x| < \xi, \\ f_2(x), & \xi \le |x| < 1, \\ f_3(x), & |x| \ge 1, \end{cases} \tag{2.6}$$

with the component functions defined as:

$$f_1(x) = -\left(\frac{\alpha_2}{\xi^2} + \alpha_5\right)x^2 + \left(\alpha_2\left(\frac{2}{\xi} + 1\right) + \alpha_4\alpha_5\right)|x|, \tag{2.7}$$

$$f_2(x) = \alpha_2(|x| + 1) + \alpha_1 \sin^2(|x|), \tag{2.8}$$

$$f_3(x) = \alpha_3|x|^\gamma. \tag{2.9}$$

Here, $0 < \xi < 1$ and $0 < \gamma < 1$ are design parameters. In this work, we select $\gamma = 2/3$. The coefficients α_1–α_5 are determined by enforcing continuity of $\Psi(x)$ and its first derivative at the transition points $|x| = \xi$ and $|x| = 1$:

$$\begin{cases} f_1(\xi) = f_2(\xi), \quad f_1'(\xi) = f_2'(\xi), \\ f_2(1) = f_3(1), \quad f_2'(1) = f_3'(1). \end{cases} \tag{2.10}$$

Solving these conditions yields:

$$\begin{aligned} \alpha_1 &= \frac{\alpha_3}{6\sin 2 - 3\sin^2 1} \approx 0.30\alpha_3, \\ \alpha_2 &= \frac{3\sin 2 - 2\sin^2 1}{6\sin 2 - 3\sin^2 1}\alpha_3 \approx 0.39\alpha_3, \\ \alpha_4 &= \frac{2\sin^2\xi - \xi\sin(2\xi)}{\sin^2\xi - \xi\sin(2\xi)}\xi, \\ \alpha_5 &= \frac{\sin^2\xi - \xi\sin(2\xi)}{\xi^2}\alpha_1, \end{aligned} \tag{2.11}$$

where $\alpha_3 > 0$ is a free design parameter. From Eq (2.11), it follows directly that $\alpha_3 > \alpha_2 > \alpha_1 > 0$ and $\alpha_4\alpha_5 > 0$.

The following property of $f(x)$ is essential for the subsequent stability analysis.

Property 1. *For the function $f(x)$ defined in* (2.6) *with parameters given by* (2.11)*, the following inequality holds:*

$$f(x) \geq \alpha_1, \quad \forall\, x : \xi \leq |x| < 1.$$

Proof. For $\xi \leq |x| < 1$, we have $f(x) = f_2(x) = \alpha_2|x| + \alpha_1 \sin^2(|x|) + \alpha_2$. Consider the auxiliary function $g(t) = \sin^2 t + t + 1$ for $t \in [0, 1)$. Its derivative is:

$$g'(t) = \sin(2t) + 1 > 0, \quad \forall t \in [0, 1),$$

since $\sin(2t) \geq -1$ for all real t. Hence, $g(t)$ is strictly increasing on $[0, 1)$, and consequently $g(t) \geq g(0) = 1$.

Rewriting $f_2(x)$ in terms of $g(|x|)$:

$$\begin{aligned} f_2(x) &= \alpha_1 \sin^2(|x|) + \alpha_2(|x| + 1) \\ &\geq \min(\alpha_1, \alpha_2)(\sin^2(|x|) + |x| + 1) \\ &= \min(\alpha_1, \alpha_2)\, g(|x|) \geq \min(\alpha_1, \alpha_2). \end{aligned}$$

From (2.11), we have $\alpha_1 \approx 0.30\alpha_3$ and $\alpha_2 \approx 0.39\alpha_3$, which implies $\min(\alpha_1, \alpha_2) = \alpha_1$. Therefore,

$$f(x) \geq \alpha_1 \quad \forall x : \xi \leq |x| < 1,$$

completing the proof. □

Remark 1. *Figures 1 and 2 illustrate the piecewise function* $\Psi(x)$ *and its derivative, respectively, with parameters* $\xi = 0.5$ *and* $\alpha_3 = 1$. *It is evident that the function and its derivative are continuous.*

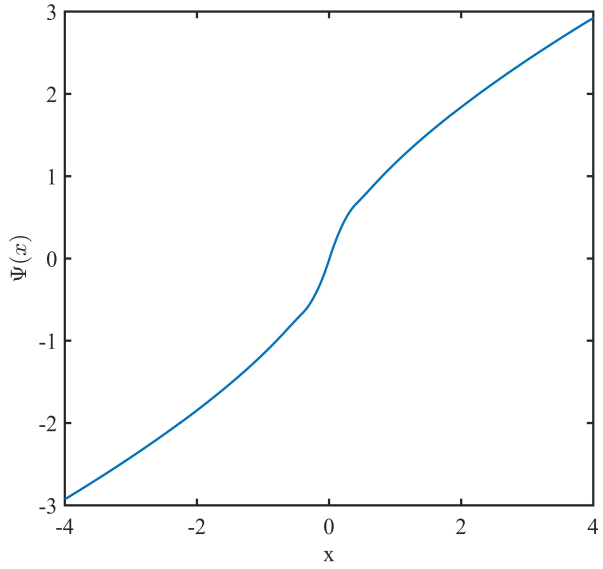

Figure 1. Graph of $\Psi(x)$.

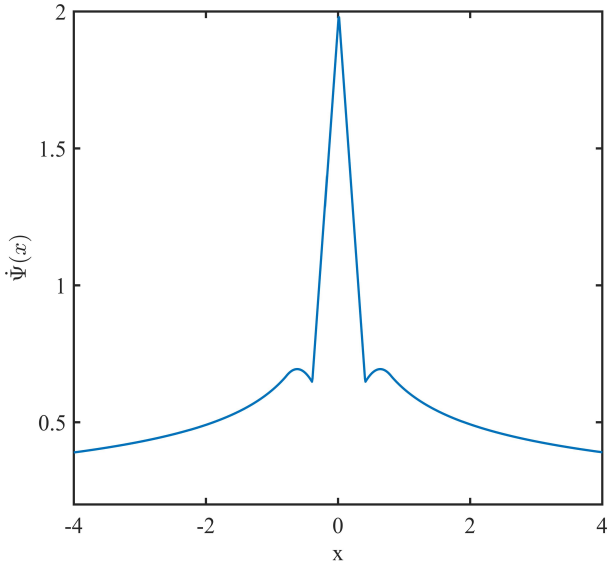

Figure 2. Graph of the derivative of $\Psi(x)$.

For the region where $|x| \geq 1$, the function is defined as $f_3(x) = \alpha_3|x|^\gamma$, with $0 < \gamma < 1$, which ensures finite-time convergence. In the region $\xi \leq |x| < 1$, the function $f_2(x)$ satisfying Property 1 is introduced to guarantee practical finite-time stability. Note that if $\xi = 0$, then at $x = 0$, we have $f_2(x) = \alpha_2$, which would cause a discontinuity of $\Psi(x)$ at the origin. To remedy this, the function $f_1(x)$ is introduced to ensure the continuity of $\Psi(x)$ and its derivative. This property is beneficial for avoiding chattering issues caused by the sign function in the subsequent sliding mode surface design. Furthermore, due to the continuity of the derivative, the singularity problem is also avoided.

Having introduced the scalar function $\Psi(x)$ and the disturbed error dynamics (2.4), we now present essential definitions and assumptions that form the theoretical foundation for the controller design.

Definition 1. *([26]) The error system* (2.4) *is said to be* finite-time stable *if for every initial condition $\mathbf{E}_0 \in \mathbb{R}^3$, there exists a settling time $T(\mathbf{E}_0) > 0$, which depends on the initial state, such that $\lim_{t \to T(\mathbf{E}_0)} \mathbf{E}(t) = \mathbf{0}$ and $\mathbf{E}(t) \equiv \mathbf{0}$ for all $t \geq T(\mathbf{E}_0)$.*

Definition 2. *([33]) The error system* (2.4) *is said to be in a* practical sliding mode *once its trajectory enters and remains within the set $\Omega = \{\mathbf{E} \in \mathbb{R}^3 : \|\mathbf{s}(t)\| < a\}$, where a is a positive constant and $\mathbf{s}(t)$ denotes the sliding variable.*

Lemma 1. *([26]) Consider the system $\dot{x} = f(x, t)$. If there exists a C^1 function $V(x) \geq 0$ such that*

$$\dot{V}(x) \leq -k_1 V^q(x) - k_2 V(x),$$

where $k_1 > 0$, $k_2 > 0$, and $0 < q < 1$, then the closed-loop system is finite-time stable, and the settling time T satisfies

$$T \leq \frac{1}{k_2(1-q)} \ln\left(1 + \frac{k_2}{k_1} V^{1-q}(x(0))\right).$$

Assumption 1. *The reference velocities v_r and ω_r are bounded and satisfy $|v_r| \leq v_m$, $g < |\omega_r| \leq \omega_m$, and $|\dot{\omega}_r| \leq \dot{\omega}_m$, where $g > 0$ is a known constant, v_m and ω_m denote the maximum allowable linear and angular velocities, respectively, and $\dot{\omega}_m$ is the maximum allowable angular acceleration.*

Assumption 2. *The posture error $\mathbf{E} = [E_x, E_y, E_\theta]^{\mathrm{T}}$ is confined within the prescribed region $\Omega_E \subset \mathbb{R}^3$ defined as:*

$$\Omega_E = \{\mathbf{E} \in \mathbb{R}^3 : |E_x| < x_m,\ |E_y| < y_m,\ |E_\theta| \leq \pi\},$$

where $x_m > 0$ and $y_m > 0$ denote the allowable position error bounds.

Assumption 3. *The unknown disturbances d_1, d_2, and their first derivatives are bounded, i.e., there exist unknown positive constants $\delta_{1i}, \delta_{2i} > 0$ such that*

$$|d_i(t)| < \delta_{1i}, \quad |\dot{d}_i(t)| < \delta_{2i}, \quad i \in \{1, 2\}. \tag{2.12}$$

3. Major results

In this section, we present a sliding mode control framework that incorporates the proposed nonlinear function to achieve finite-time trajectory tracking for robotic systems. The controller architecture is developed through three integral components: First, a finite-time disturbance observer

is constructed to provide real-time estimates of unknown disturbances; second, a novel nonsingular sliding mode control scheme is developed based on the observer to ensure finite-time convergence of tracking errors while avoiding singularity issues; and third, the control framework is enhanced with event-triggered mechanisms to establish an efficient event-triggered sliding mode control architecture. The stability of the resulting closed-loop system is rigorously analyzed using Lyapunov stability theory and Lipschitz continuity analysis.

3.1. Disturbance observer design

To ensure finite-time convergence of the tracking error, the sliding manifold is designed as follows:

$$\mathbf{s} = \begin{bmatrix} s_1 \\ s_2 \end{bmatrix} = \begin{bmatrix} E_x - \lambda\omega_r\Psi(E_y) \\ E_\theta \end{bmatrix}, \tag{3.1}$$

where $\lambda > 0$ represents a tunable control parameter.

Based on the error dynamics in (2.4), the time derivative of the sliding variable $\mathbf{s}$ is derived as:

$$\begin{aligned} \dot{\mathbf{s}} &= \begin{bmatrix} \dot{E}_x - \lambda\dot{\omega}_r\Psi(E_y) - \lambda\omega_r\dot{\Psi}(E_y)\dot{E}_y \\ \dot{E}_\theta \end{bmatrix} \\ &= \mathbf{J}(\mathbf{E})\mathbf{H}(\mathbf{E}) + \mathbf{B}(\mathbf{E})\mathbf{V} + \mathbf{P}(\mathbf{E}) + \Delta, \end{aligned} \tag{3.2}$$

with the matrix components defined as:

$$\begin{aligned} &\mathbf{J}(\mathbf{E}) = \begin{bmatrix} 1 & a & 0 \\ 0 & 0 & 1 \end{bmatrix}, \quad \mathbf{H}(\mathbf{E}) = \begin{bmatrix} v_r\cos E_\theta \\ v_r\sin E_\theta \\ \omega_r \end{bmatrix}, \quad \mathbf{B}(\mathbf{E}) = \begin{bmatrix} -1 & b \\ 0 & -1 \end{bmatrix}, \\ &\mathbf{P}(\mathbf{E}) = \begin{bmatrix} -\lambda\dot{\omega}_r\Psi(E_y) \\ 0 \end{bmatrix}, \quad \Delta = \mathbf{B}(\mathbf{E})\mathbf{d}, \quad \mathbf{d} = \begin{bmatrix} d_1 \\ d_2 \end{bmatrix}, \end{aligned} \tag{3.3}$$

where the coefficients a and b are given by:

$$a = -\lambda\omega_r\Pi(E_y), \quad b = E_y + \lambda\omega_r E_x\Pi(E_y), \tag{3.4}$$

and the nonlinear function $\Pi(E_y)$ is piecewise defined as:

$$\Pi(E_y) = \begin{cases} -2\left(\dfrac{\alpha_2}{\xi^2} + \alpha_5\right)|E_y| + \alpha_2\left(\dfrac{2}{\xi} + 1\right) + \alpha_4\alpha_5, & |E_y| < \xi, \\ \alpha_1\sin(2|E_y|) + \alpha_2, & \xi \le |E_y| < 1, \\ \dfrac{2}{3}\alpha_3|E_y|^{-1/3}, & |E_y| \ge 1. \end{cases} \tag{3.5}$$

External disturbances introduce the uncertain term Δ in (3.2). To eliminate their effects, a disturbance observer is designed using the following structure:

$$\begin{cases} \dot{\hat{\mathbf{s}}} = \mathbf{J}(\mathbf{E})\mathbf{H}(\mathbf{E}) + \mathbf{B}(\mathbf{E})\mathbf{V} + \mathbf{P}(\mathbf{E}) + \hat{\Delta}, \\ \boldsymbol{\sigma} = \mathbf{e} + \displaystyle\int_0^t \boldsymbol{\kappa}_1\boldsymbol{\varphi}_1(\tau)d\tau, \\ \hat{\Delta} = \boldsymbol{\kappa}_1\boldsymbol{\varphi}_1 + \boldsymbol{\kappa}_2\boldsymbol{\varphi}_2 + \mathbf{r}\boldsymbol{\varphi}_3, \\ \hat{\mathbf{d}} = \mathbf{B}^{-1}(\mathbf{E})\hat{\Delta}, \end{cases} \tag{3.6}$$

where $\mathbf{e} = \mathbf{s} - \hat{\mathbf{s}}$ denotes the estimation error, with $\hat{\mathbf{s}}$ being the estimated state, $\hat{\Delta}$ representing the uncertain term estimate, and $\hat{\mathbf{d}}$ standing for the disturbance estimate. The sliding variable vector $\boldsymbol{\sigma} = [\sigma_1, \sigma_2]^\top$ incorporates nonlinear functions $\boldsymbol{\varphi}_1 = [\varphi_{11}, \varphi_{12}]^\top$ where $\varphi_{1i} = \Psi(e_i)$, $\boldsymbol{\varphi}_2 = [\varphi_{21}, \varphi_{22}]^\top$ with $\varphi_{2i} = \text{sat}(\sigma_i)$, and $\boldsymbol{\varphi}_3 = [\varphi_{31}, \varphi_{32}]^\top$ where $\varphi_{3i} = \text{sat}(\sigma_i)$. The gain matrices are diagonal with $\boldsymbol{\kappa}_1 = \text{diag}\{\kappa_{11}, \kappa_{12}\}$, $\boldsymbol{\kappa}_2 = \text{diag}\{\kappa_{21}, \kappa_{22}\}$, and $\mathbf{r} = \text{diag}\{r_1, r_2\}$, satisfying $\kappa_{1i}, \kappa_{2i} > 0$ and $r_i > \bar{\Delta}_i$. The function $\text{sat}(x)$ is expressed as

$$\text{sat}(x) = \begin{cases} \text{sign}(x), & \text{if } |x| \geq \iota, \\ \dfrac{2}{1 + \exp\left(\dfrac{-kx}{x^2 - \iota^2}\right)}, & \text{if } |x| < \iota, \end{cases}$$

and $k, \iota > 0$ are design parameters.

Remark 2. *([23]) A saturation function* $\text{sat}(x)$ *is introduced to replace the sign function* $\text{sign}(x)$*, thereby effectively mitigating system chattering. The proposed function is continuous at the boundary points* $x = \iota$ *and* $x = -\iota$*, satisfying*

$$\lim_{x \to \iota^-} \text{sat}(x) = 1$$

and

$$\lim_{x \to -\iota^+} \text{sat}(x) = -1.$$

By choosing an appropriate gain k *and a sufficiently small boundary parameter* ι*, the saturation function* $\text{sat}(x)$ *yields a smooth approximation of the discontinuous* $\text{sign}(x)$ *function.*

Remark 3. *Under Assumptions 1–3 and condition* (3.4)*, parameter* b *satisfies* $|b| \leq \bar{b}$ *for some known constant* $\bar{b} > 0$ *(see Appendix). Moreover, the disturbance* d_i *is bounded by* $|d_i| \leq \bar{d}_i$ *in accordance with Assumption 3. As a result, the uncertain term* $\Delta = \mathbf{Bd}$ *remains bounded, satisfying* $|\Delta_i| \leq \bar{\Delta}_i$*. These boundedness properties ensure the existence of a control gain* $\mathbf{r}$ *such that each component fulfills* $r_i > \bar{\Delta}_i$*.*

The time derivative of $\boldsymbol{\sigma}$ yields:

$$\dot{\boldsymbol{\sigma}} = \dot{\mathbf{e}} + \boldsymbol{\kappa}_1 \boldsymbol{\varphi}_1 = \dot{\mathbf{s}} - \dot{\hat{\mathbf{s}}} + \boldsymbol{\kappa}_1 \boldsymbol{\varphi}_1 = \Delta - \hat{\Delta} + \boldsymbol{\kappa}_1 \boldsymbol{\varphi}_1 = \Delta - \boldsymbol{\kappa}_2 \boldsymbol{\varphi}_2 - \mathbf{r} \boldsymbol{\varphi}_3 \tag{3.7}$$

where $\dot{\boldsymbol{\sigma}} = [\dot{\sigma}_1, \dot{\sigma}_2]^\top$ and $\dot{\mathbf{e}} = \dot{\mathbf{s}} - \dot{\hat{\mathbf{s}}} = \Delta - \hat{\Delta}$ represent the derivative vector of sliding variable and the estimation error dynamics, respectively.

Theorem 1. *Consider the mobile robot error system* (2.4) *under Assumption 3. The proposed disturbance observer* (3.6) *ensures that the estimation errors converge to the residual set* $\Omega = \{\tilde{d}_i \mid |\tilde{d}_i| \leq \gamma_i\}, (i = 1, 2)$*, within a settling time* T_{obs}*, where* $\gamma_1 = \Gamma_1 + \bar{b}\Gamma_2$*,* $\gamma_2 = \Gamma_2$ *and* $\Gamma_i = \kappa_{1i}\left(\alpha_2 |\xi| + \alpha_1 \sin^2(|\xi|) + \alpha_2\right)$ *for* $i = 1, 2$

$$\begin{aligned} &T_{\text{obs}} \leq T_{\text{or}} + T_{\text{os}}, \quad T_{\text{or}} \leq \frac{\sqrt{2} V_0^{1/2}(\boldsymbol{\sigma}_0)}{\lambda_{\min}(\boldsymbol{\kappa}_2)}, \\ &T_{\text{os}} = \max\{t_{31}, t_{32}\}, \quad t_{3i} = \frac{6 V_{1i}^{1/6}(e_i(0))}{(\kappa_{1i}\alpha_3 - Q_i) 2^{5/6}} + \frac{1}{\kappa_{1i}\alpha_1 - Q_i}. \end{aligned} \tag{3.8}$$

Here, $Q_i = \bar{\Delta}_i + \kappa_{2i} + r_i$*,* $\kappa_{1i} > \max(\frac{Q_i}{\alpha_1}, \frac{Q_i}{\alpha_3})$*,* $\kappa_{2i} > 0$ *and* $V_0(\boldsymbol{\sigma}_0)$*,* $V_{1i}(e_i(0))$ *represent the initial values of the corresponding Lyapunov functions.*

Proof. Define the Lyapunov function:

$$V_0 = \frac{1}{2}\boldsymbol{\sigma}^\top \boldsymbol{\sigma}. \tag{3.9}$$

When $|\sigma_i| < \iota$, taking its time derivative and substituting (3.7) yields:

$$\begin{aligned} \dot{V}_0(t) = \boldsymbol{\sigma}^\top \dot{\boldsymbol{\sigma}} = \boldsymbol{\sigma}^\top (\Delta - \boldsymbol{\kappa_2}\boldsymbol{\varphi}_2 - \boldsymbol{r}\boldsymbol{\varphi}_3) \leq \sum_{i=1}^{2} -\kappa_{2i}|\sigma_i| - (r_i - \bar{\Delta}_i)|\sigma_i| \\ \leq -\lambda_{\min}(\boldsymbol{\kappa_2})\,\|\boldsymbol{\sigma}\| \leq -\sqrt{2}\lambda_{\min}(\boldsymbol{\kappa_2}) V_0^{\frac{1}{2}}. \end{aligned} \tag{3.10}$$

The sliding variable $\boldsymbol{\sigma}$ is finite-time practically stable and will converge to $|\sigma_i| < \iota$. The upper bound of the reaching time is given by:

$$T_{\text{or}} \leq \frac{\sqrt{2} V_0^{\frac{1}{2}}(\boldsymbol{\sigma}_0)}{\lambda_{\min}(\boldsymbol{\kappa}_2)}. \tag{3.11}$$

When the system state moves onto the sliding surface, we have $\dot{\mathbf{e}} = -\boldsymbol{\kappa}_1\boldsymbol{\varphi}_1 + \dot{\boldsymbol{\sigma}}$ and $|\dot{\sigma}_i| \leq \bar{\Delta}_i + \kappa_{2i} + r_i \triangleq Q_i$. Choose a new Lyapunov function as:

$$V_1 = \sum_{i=1}^{2} V_{1i} = \frac{1}{2}\sum_{i=1}^{2} e_i^2.$$

Taking the time derivative of V_{1i} yields:

$$\dot{V}_{1i} = e_i \dot{e}_i = -\kappa_{1i}|e_i| f(e_i) + e_i \dot{\sigma}_i. \tag{3.12}$$

For $|e_i| \geq 1$, from (2.6), we obtain:

$$\dot{V}_{1i} \leq -\kappa_{1i}|e_i| f(e_i) + |\dot{\sigma}_i||e_i| \leq -(\kappa_{1i}\alpha_3 - Q_i)|e_i|^{\frac{5}{3}} \leq -2^{\frac{5}{6}}(\kappa_{1i}\alpha_3 - Q_i) V_{1i}^{\frac{5}{6}}. \tag{3.13}$$

Similarly, we derive the following inequality:

$$\int_0^{t_{2i}} \frac{dV_{1i}}{V_{1i}^{\frac{5}{6}}} \leq -2^{\frac{5}{6}}(\kappa_{1i}\alpha_3 - Q_i) \int_0^{t_{2i}} d\tau. \tag{3.14}$$

Solving this inequality gives:

$$t_{2i} \leq \frac{6 V_{1i}^{\frac{1}{6}}(0)}{(\kappa_{1i}\alpha_3 - Q_i) 2^{\frac{5}{6}}}. \tag{3.15}$$

For $\xi \leq |e_i| < 1$, according to Property 1, we have:

$$\dot{V}_{1i} \leq -\kappa_{1i}|e_i| f(e_i) + |\dot{\sigma}_i||e_i| \leq -(\kappa_{1i}\alpha_1 - Q_i)|e_i| \leq -\sqrt{2}(\kappa_{1i}\alpha_1 - Q_i) V_{1i}^{\frac{1}{2}}. \tag{3.16}$$

Then we obtain the following inequality:

$$\int_{t_{2i}}^{t_{3i}} \frac{dV_{1i}}{V_{1i}^{\frac{1}{2}}} \leq -\sqrt{2}(\kappa_{1i}\alpha_1 - Q_i) \int_{t_{2i}}^{t_{3i}} d\tau.$$

Solving this equation gives:

$$t_{3i} \leq t_{2i} + \frac{1}{\kappa_{1i}\alpha_1 - Q_i}. \tag{3.17}$$

Finally, based on (3.11), (3.15) and (3.17), the total convergence time is:

$$T_{\text{obs}} \leq T_{\text{or}} + T_{\text{os}}, \quad T_{\text{os}} = \max\{t_{31}, t_{32}\}, \quad t_{3i} = \frac{6V_{1i}^{\frac{1}{6}}(e_i(0))}{(\kappa_{1i}\alpha_3 - Q_i)2^{\frac{5}{6}}} + \frac{1}{\kappa_{1i}\alpha_1 - Q_i}. \tag{3.18}$$

The following analysis demonstrates that the disturbance estimation error $\tilde{d}_i$ converges to a residual set. According to the properties of the nonlinear function (2.6), when $t \geq T_{\text{obs}}$, the estimation error e_i converges to the region $|e_i| < \xi$.

From (3.7) and (3.12), the derivative of the error variable satisfies:

$$\dot{e}_i = \Delta_i - \hat{\Delta}_i = -\kappa_{1i}\Psi(e_i) + \dot{\sigma}_i. \tag{3.19}$$

Combining this with (2.6) yields:

$$|\dot{e}_i| \leq \kappa_{1i}|f(e_i)| + |\dot{\sigma}_i| \leq \kappa_{1i}|f_2(\xi)| + Q_i = \kappa_{1i}\left(\alpha_2|\xi| + \alpha_1 \sin^2(|\xi|) + \alpha_2\right) + Q_i \triangleq \Gamma_i. \tag{3.20}$$

Based on the relationship between the disturbance $\boldsymbol{d}$ and the uncertainty term $\boldsymbol{\Delta}$, the convergence region of the disturbance estimation error $\tilde{\boldsymbol{d}}$ can be derived as:

$$\begin{aligned} &|\tilde{d}_1| \leq \Gamma_1 + \bar{b}\Gamma_2 \triangleq \gamma_1, \\ &|\tilde{d}_2| \leq \Gamma_2 \triangleq \gamma_2. \end{aligned} \tag{3.21}$$

This completes the proof. □

Remark 4. *By employing a piecewise continuous function, the sliding mode disturbance observer developed in this study eliminates the chattering phenomenon present in the methods of [22–24]. Once the observer state error reaches the sliding surface, it converges to and remains within a predefined region in finite time, thereby achieving practical finite-time stability. By adjusting parameters ξ and α_3 in Eq* (2.6)*, the convergence region of the disturbance estimation error can be flexibly regulated. Consequently, compared to existing approaches, the proposed disturbance observer achieves higher estimation accuracy.*

In Eq (3.10), the robust term $\mathbf{r}\boldsymbol{\varphi}_3$ is employed to compensate for the unknown disturbances $\boldsymbol{\Delta}$, where the gain matrix $\mathbf{r} = \text{diag}\{r_1, r_2\}$ must satisfy condition $r_i > \bar{\Delta}_i$ according to Assumption 3. However, in practical applications, these disturbance upper bounds $\bar{\Delta}_i$ are generally unknown. To overcome this limitation, we design an adaptive mechanism based on the equivalent control principle from sliding mode theory to estimate the upper bounds of the disturbance. When the ideal sliding mode condition $\dot{\boldsymbol{\sigma}}_i = \mathbf{0}$ is satisfied, the equivalent control $u_{\text{eq}i}$ must fully counteract the disturbance Δ_i to maintain the sliding motion, and its theoretical value is determined by the term $-\boldsymbol{\kappa}_2\boldsymbol{\varphi}_2 - \mathbf{r}\boldsymbol{\varphi}_3$ in Eq (3.7). It should be noted that the equivalent control, as a theoretical concept, is unknown in practice and requires estimation via a first-order filter.

For practical implementation, we design a nonlinear first-order filter to estimate this equivalent control:

$$\dot{\bar{u}}_{\text{eq}i} = \mu_{1i}\Psi(-\kappa_{2i}\varphi_{2i} - r_i\varphi_{3i} - \bar{u}_{\text{eq}i}), \quad i = 1, 2 \tag{3.22}$$

where $\bar{u}_{eqi}$ is the estimation of u_{eqi}, $\bar{\mathbf{u}}_{eq} = [\bar{u}_{eq1}, \bar{u}_{eq2}]^\top$, $\boldsymbol{\mu}_1 = [\mu_{11}, \mu_{12}]$ with $\mu_{1i} > 0$ for $i = 1, 2$.

Then an adaptive law is given as:

$$\begin{cases} r_i(t) = r_{0i} + \rho_i(t), \\ \dot{\rho}_i(t) = -\mu_{2i}\Psi(\zeta_i), \\ \zeta_i = r_i(t) - \dfrac{|\bar{u}_{eqi}|}{\mu_{3i}} - \varepsilon_i, \end{cases} \tag{3.23}$$

where $\mathbf{r}(t) = \text{diag}\{r_1(t), r_2(t)\}$, $\mathbf{r}_0 = [r_{01}, r_{02}]^\top$, $\boldsymbol{\zeta}(t) = [\zeta_1(t), \zeta_2(t)]^\top$, with r_{01}, r_{02}, μ_{21}, μ_{22} being positive constants, $0 < \mu_{3i} < 1$, and ε_i being a small positive constant.

Theorem 2. *Consider the disturbance observer introduced in Eq* (3.6)*. If the low-pass filter is chosen as* (3.22) *and the adaptive mechanism is designed as* (3.23)*, then $r_i(t) > |\Delta_i|$ can be guaranteed.*

Proof. Differentiating $\zeta_i(t)$ with respect to time yields:

$$\dot{\zeta}_i(t) = -\mu_{2i}\Psi(\zeta_i(t)) - \frac{\varphi_i(t)}{\mu_{3i}} \tag{3.24}$$

where $\varphi_i(t) = \dot{\bar{u}}_{eqi}$, satisfying $|\varphi_i(t)| < k_\phi \delta_{2i}$ with $k_\phi > 1$ as a designed safety margin.

Consider the Lyapunov function candidate:

$$V_r = \frac{1}{2}\zeta_i^2.$$

Taking its time derivative and substituting (3.24) gives:

$$\begin{aligned} \dot{V}_r &= -\zeta_i \left(\mu_{2i}\Psi(\zeta_i(t)) + \frac{\varphi_i(t)}{\mu_{3i}} \right) \\ &\leq -\mu_{2i}|\zeta_i| f(\zeta_i) + \frac{k_\phi \delta_{2i}}{\mu_{3i}}|\zeta_i| \\ &\leq -|\zeta_i| \left(\mu_{2i} f(\zeta_i) - \frac{k_\phi \delta_{2i}}{\mu_{3i}} \right). \end{aligned} \tag{3.25}$$

When $|\zeta_i(t)| > \chi_i$, where

$$f(\chi_i) = \frac{k_\phi \delta_{2i}}{\mu_{2i}\mu_{3i}},$$

such that $f(\zeta_i) - f(\chi_i) > 0$ holds, Eq (3.25) satisfies $\dot{V}_r < 0$. Therefore, ζ_i converges to and remains within a neighborhood of zero $\varpi_i = \{\zeta_i(t) : |\zeta_i| \leq \chi_i\}$.

This implies the existence of a positive constant ε_i satisfying $|\zeta_i| < \dfrac{\varepsilon_i}{2}$, from which it follows that:

$$|\zeta_i| = \left| r_i(t) - \frac{|u_{eqi}|}{\mu_{3i}} - \varepsilon_i \right| < \frac{\varepsilon_i}{2}. \tag{3.26}$$

Furthermore, from (3.26) and the condition $0 < \mu_{3i} < 1$, it follows that:

$$|r_i(t)| > \frac{|\bar{u}_{eqi}|}{\mu_{3i}} + \frac{\varepsilon_i}{2} > |\Delta_i| + \frac{\varepsilon_i}{2} > |\Delta_i|. \tag{3.27}$$

From (3.23), it is straightforward to show:

$$|r_i(t)| < |\zeta_i| + \frac{|\bar{u}_{\mathrm{eq}i}|}{\mu_{3i}} + |\varepsilon_i| < |\zeta_i| + \frac{\delta_{1i}}{\mu_{3i}} + |\varepsilon_i|. \tag{3.28}$$

Therefore, $r_i(t)$ remains bounded. Furthermore, from (3.23) and (3.26), it follows directly that $\rho_i(t)$ and ζ_i are bounded. This completes the proof. □

Remark 5. *The designed adaptive scheme is motivated by [34]. The adaptive mechanism* (3.23) *utilizes the low-pass filter* (3.22) *to estimate u_{eqi}, thereby enabling real-time estimation of the disturbance bounds and enhancing the robustness of the disturbance observer. According to* (3.23)*, the estimated value of $r_i(t)$ will gradually increase until the system reaches the sliding mode, after which it decreases and converges to a safe bound. Parameter $r_{0i} > 0$ is used to ensure that the initial value of $r_i(t)$ is positive. The coefficients ε_i and μ_{3i} serve as a safety factor and a scaling factor, respectively, adjusting the magnitude of the upper-bound estimation function $r_i(t)$. Increasing ε_i or decreasing μ_{3i} will enlarge $r_i(t)$, thereby yielding a more reliable estimate of the upper bound. By adjusting the parameters r_{0i}, ε_i, and μ_{3i}, different safety margins can be achieved to meet practical engineering requirements.*

3.2. Finite-time sliding mode controller design

In this section, we present a disturbance-observer-based sliding mode control scheme that ensures finite-time convergence of the robot's trajectory tracking error.

The proposed controller is designed as:

$$\mathbf{V}_c = -\mathbf{B}^{-1}(\mathbf{E})\left(\mathbf{J}(\mathbf{E})\mathbf{H}(\mathbf{E}) + \boldsymbol{\beta}\mathrm{sign}(\mathbf{s}) + k\mathbf{s} + \mathbf{P}(\mathbf{E}) + \frac{k_s^2\mathbf{s}}{k_s\|\mathbf{s}\| + \exp(-\lambda_s t)}\right) - \hat{\mathbf{d}}, \tag{3.29}$$

where $\boldsymbol{\beta} = \mathrm{diag}\{\beta_1, \beta_2\}$ ($\beta_i > \Gamma_i$, $i = 1, 2$) is the controller gain matrix, Γ_i, $i = 1, 2$ are bounds on estimation errors of the disturbance observer. $k, k_s > 0$ are design parameters, and $\hat{\mathbf{d}}$ denotes the estimated unknown disturbances.

Theorem 3. *Consider the posture tracking error system* (2.4) *under the disturbance observer* (3.6)*, adaptive mechanism* (3.23)*, sliding surface* (3.1)*, and controller* (3.29)*. The mobile robot's attitude tracking error $\mathbf{E} = [E_x, E_y, E_\theta]^{\mathrm{T}}$ converges to a neighborhood of zero within a finite time T_c bounded by:*

$$\begin{aligned} &T_c \le T_{\mathrm{obs}} + T_{\mathrm{rc}} + T_{\mathrm{rs}}, \\ &T_{\mathrm{rc}} = \frac{2}{K_2}\ln\left(1 + \frac{K_2}{K_1}V_3^{1/2}(\boldsymbol{s}_0)\right), T_{\mathrm{rs}} = \frac{1}{\lambda g^2}\left(\frac{6V_4^{1/6}(E_y(0))}{2^{5/6}} + \frac{1}{\alpha_1}\right), \end{aligned} \tag{3.30}$$

where $K_1 = \sqrt{2}\min(\beta_1 - \gamma_1, \beta_2 - \gamma_2)$, $K_2 = 2k$, and T_{obs} denotes the convergence time of the disturbance observer.

Proof. Consider the Lyapunov function candidate:

$$V_3 = \frac{1}{2}\mathbf{s}^{\mathrm{T}}\mathbf{s}.$$

Taking its time derivative along the sliding variable $\mathbf{s}$ yields:

$$\dot{V}_3 = \mathbf{s}^{\mathrm{T}}\dot{\mathbf{s}} = \mathbf{s}^{\mathrm{T}}(\mathbf{J}(\mathbf{E})\mathbf{H}(\mathbf{E}) + \mathbf{B}(\mathbf{E})\mathbf{V} + \mathbf{P}(\mathbf{E}) + \Delta). \tag{3.31}$$

Substituting the control law (3.29) and using the Cauchy-Schwarz inequality gives:

$$\begin{aligned}
\dot{V}_3 &= \mathbf{s}^{\mathrm{T}}\left(-\frac{k_s^2\mathbf{s}}{k_s\|\mathbf{s}\| + \exp(-\lambda_s t)} - \boldsymbol{\beta}\mathrm{sign}(\mathbf{s}) - k\mathbf{s} + \mathbf{B}(\mathbf{E})(\mathbf{d} - \hat{\mathbf{d}})\right) \\
&= -\beta_1|s_1| - \beta_2|s_2| - k\|\boldsymbol{s}\|^2 - \frac{k_s^2\|\mathbf{s}\|^2}{k_s\|\mathbf{s}\| + \exp(-\lambda_s t)} + \mathbf{s}^{\mathrm{T}}\tilde{\Delta} \\
&\leq -(\beta_1 - |\tilde{\Delta}_1|)|s_1| - (\beta_2 - |\tilde{\Delta}_2|)|s_2| - k\|\boldsymbol{s}\|^2 - \frac{k_s^2\|\mathbf{s}\|^2}{k_s\|\mathbf{s}\| + \exp(-\lambda_s t)} \\
&\leq -(\beta_1 - \gamma_1)|s_1| - (\beta_2 - \gamma_2)|s_2| - k\|\boldsymbol{s}\|^2 \\
&\leq -\sqrt{2}\min(\beta_1 - \gamma_1, \beta_2 - \gamma_2)V_3^{1/2} - 2kV_3 \\
&\leq -K_1V_3^{1/2} - K_2V_3,
\end{aligned} \tag{3.32}$$

where $K_1 = \sqrt{2}\min(\beta_1 - \gamma_1, \beta_2 - \gamma_2)$, $K_2 = 2k$.

According to Lemma 1, the sliding variable $\mathbf{s}$ is finite-time stable, and its convergence time satisfies the following bound:

$$T_{\mathrm{rc}} = \frac{2}{K_2}\ln\left(1 + \frac{K_2}{K_1}V_3^{\frac{1}{2}}(\boldsymbol{s}_0)\right). \tag{3.33}$$

When $\mathbf{s} = \mathbf{0}$, it follows from (3.1) and (2.4) that:

$$\begin{cases}
E_\theta = \theta_r - \theta = 0, \\
E_x = \lambda\omega_r\Psi(E_y), \\
\omega + d_2 = \omega_r.
\end{cases} \tag{3.34}$$

Combining the controller (3.29) with the attitude error dynamics (2.4), derivative $\dot{E}_y$ is given by:

$$\dot{E}_y = -\lambda\omega_r^2\Psi(E_y). \tag{3.35}$$

Consider the scalar Lyapunov function:

$$V_4 = \frac{1}{2}E_y^2.$$

Taking its time derivative and substituting (3.35) yields:

$$\dot{V}_4 = -\lambda\omega_r^2|E_y|f(E_y). \tag{3.36}$$

Case 1. ($|E_y| \geq 1$): Combining (2.6) and (3.36) gives:

$$\dot{V}_4 = -\lambda\omega_r^2|E_y|^{5/3} = -2^{5/6}\lambda\omega_r^2V_4^{5/6}, \tag{3.37}$$

which can be rewritten as:

$$\int_0^{t_1}\frac{dV_4}{V_4^{5/6}} = -2^{5/6}\lambda\omega_r^2\int_0^{t_1}d\tau.$$

Based on Assumption 1, we obtain:

$$t_1 = \frac{6\left(V_4^{1/6}(E_y(t_1)) - V_4^{1/6}(E_y(0))\right)}{-2^{5/6}\lambda\omega_r^2} \leq \frac{6V_4^{1/6}(E_y(0))}{2^{5/6}\lambda g^2}. \tag{3.38}$$

Case 2. ($\xi \leq |E_y| < 1$): According to Property 1, we have:

$$\dot{V}_4 \leq -\lambda\alpha_1\omega_r^2|E_y| \leq -\sqrt{2}\lambda\alpha_1\omega_r^2 V_4^{1/2}. \tag{3.39}$$

Thus, we obtain:

$$\int_{t_1}^{t_2} \frac{dV_4}{V_4^{1/2}} = -\sqrt{2}\lambda\alpha_1\omega_r^2 \int_{t_1}^{t_2} d\tau.$$

Considering that $V_4(t) < \frac{1}{2}$ for $t > t_1$, we derive:

$$t_2 \leq t_1 + \frac{2\left(V_4^{1/2}(E_y(t_2)) - V_4^{1/2}(E_y(t_1))\right)}{-\sqrt{2}\lambda\alpha_1\omega_r^2} \leq t_1 + \frac{1}{\lambda\alpha_1 g^2}. \tag{3.40}$$

Combining (3.33), (3.38), and (3.40), the convergence time of the attitude error satisfies:

$$T_c \leq T_{\text{obs}} + T_{\text{rc}} + T_{\text{rs}}, \tag{3.41}$$

where

$$T_{\text{rc}} = \frac{2}{K_2}\ln\left(1 + \frac{K_2}{K_1}V_3^{\frac{1}{2}}(\boldsymbol{s}_0)\right),$$
$$T_{\text{rs}} = \frac{1}{\lambda g^2}\left(\frac{6V_4^{1/6}(E_y(0))}{2^{5/6}} + \frac{1}{\alpha_1}\right),$$

and T_{obs} represents the stabilization time of the disturbance observer.

When the system is stable, it holds that $|E_y| < \xi$ and the sliding variable $\boldsymbol{s}$ is bounded. According to (3.4), (3.5), and Assumptions 1 and 2, both a and b are bounded. Then, from (3.29) and (3.3), the boundedness of $\mathbf{V}_c$ follows directly. This completes the proof. □

Remark 6. *Through the use of piecewise functions, the sliding surface proposed in this paper avoids the singularity problem in traditional finite-time sliding mode control. For $|E_y| \geq 1$, we have $s_1 = \alpha_3|E_y|^{2/3}$, which ensures finite-time stability of the sliding variable. For $\xi \leq |E_y| < 1$, we have $s_1 = \alpha_2|E_y| + \alpha_1\sin^2(|E_y|) + \alpha_2$, which guarantees practical finite-time stability. For $|E_y| < \xi$, the quadratic function ensures continuity of s_1 and its derivative at the origin, thereby mitigating chattering.*

Remark 7. *Reference [26] developed a finite-time sliding mode control scheme for mobile robot trajectory tracking, where the convergence time is bounded by:*

$$t \leq \frac{\sqrt{2}V^{1/2}(0)}{\eta_4}, \quad \eta_4 = \frac{v_r|y_e|}{\sqrt{1+y_e^2}},$$

which explicitly depends on the attitude tracking error y_e. By contrast, the settling time T_c of the proposed controller is determined by the initial posture error and the lower bound g of the reference angular velocity ω_r, which highlights a distinct characteristic compared to existing control schemes.

Remark 8. *Under the proposed control law, the tracking error E_y enters the neighborhood $\{E_y : |E_y| < \xi\}$ within finite time T_c and subsequently converges asymptotically to zero, as ensured by the negative definiteness of $\dot{V}_4$. According to Eq* (3.34)*, the attitude error E_x converges to the region*

$$|E_x| < \lambda\omega_m \left(\alpha_2|\xi| + \alpha_1 \sin^2 |\xi| + \alpha_2\right)$$

within the same settling time T_c, and asymptotically approaches zero as E_y converges. As a result, high-precision trajectory tracking can be achieved by adjusting the controller parameters, thereby highlighting another merit of the proposed control scheme compared to prior works.

3.3. Event-triggered controller design

Building upon the disturbance-observer-based finite-time sliding mode control framework established in Section 3.2, an event-triggered mechanism is introduced to alleviate communication and computational demands while preserving closed-loop stability.

As illustrated in Figure 3, the controller communicates with the plant through a wireless network. The transmitted state vector is denoted by $\check{\mathbf{E}} = [\check{E}_x, \check{E}_y, \check{E}_\theta]^\mathsf{T}$.

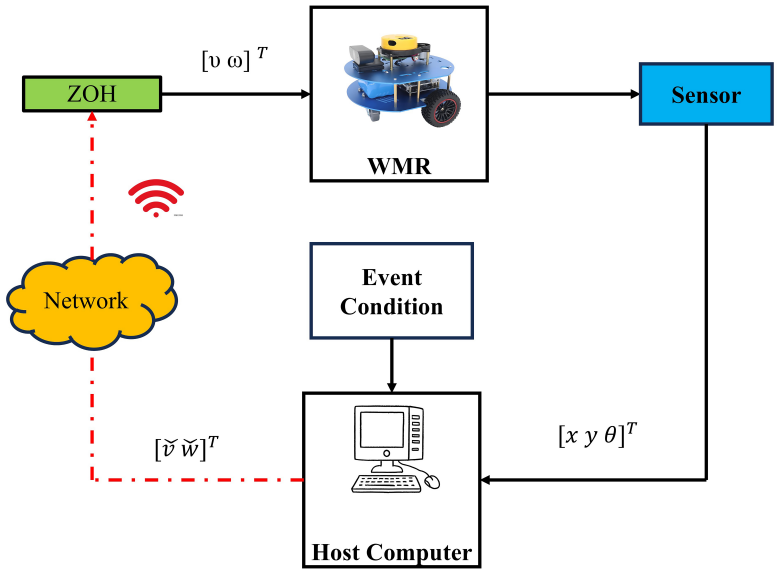

Figure 3. Closed-loop control system architecture with event-triggering strategy.

Triggering instants $t_k \in \mathbb{R}^+$ $(k \in \mathbb{N})$ are determined by violations of the triggering condition, with control signals maintained constant between consecutive events via a zero-order hold. The event-triggered controller is formulated as:

$$\mathbf{V}_c = -\mathbf{B}^{-1}(\check{\mathbf{E}}) \left(\mathbf{J}(\check{\mathbf{E}})\mathbf{H}(\check{\mathbf{E}}) + \bar{\boldsymbol{\beta}}\text{sign}(\check{\mathbf{s}}) + \check{\boldsymbol{\vartheta}} + k\check{\mathbf{s}} + \mathbf{P}(\check{\mathbf{E}})\right) - \check{\hat{\mathbf{d}}}, \tag{3.42}$$

where $\check{\mathbf{s}}$ represents the sampled sliding variable,

$$\check{\boldsymbol{\vartheta}} = \frac{k_s^2 \check{\mathbf{s}}}{k_s\|\check{\mathbf{s}}\| + \exp(-\lambda_s t_k)}.$$

$\bar{\boldsymbol{\beta}} = \text{diag}\{\bar{\beta}_1(\check{E}_x), \bar{\beta}_2\}$ is the gain matrix to be designed, and $k > 0$ is a design parameter.

The measurement error is defined as:

$$\eta(t) \triangleq |E_x - \check{E}_x| + \frac{2\lambda\omega_m\alpha_3}{\xi^2}|E_y - \check{E}_y| + |E_\theta - \check{E}_\theta| + |\hat{d}_1 - \check{\hat{d}}_1| + |\hat{d}_2 - \check{\hat{d}}_2|, \tag{3.43}$$

where λ, α_3 and ξ are defined in (2.6).

Theorem 4. *Consider the error system* (2.4) *with sliding variable* (3.1) *under the event-triggered control law* (3.42)*, the trigger condition*

$$\eta(t) \leq \delta, \tag{3.44}$$

where $\delta > 0$ is a positive constant to be selected. and control gains as follows:

$$\begin{aligned}
\bar{\beta}_1(\check{E}_x) \geq & \left\{ v_m \left(1 + 2\sqrt{1 + (\frac{2\lambda\omega_m\alpha_3}{\xi^2})^2} \right) + (\omega_m + k_s + \bar{\beta}_2) \left(\frac{\xi^2}{2\lambda\omega_m\alpha_3} + \frac{2\lambda\omega_m\alpha_3}{\xi}(1 + \frac{|\check{E}_x|}{\xi}) \right) \right. \\
& \left. + \frac{\xi\dot{\omega}_m}{\omega_m} + \gamma_1 + y_m + \frac{2\lambda\omega_m\alpha_3 x_m}{\xi} \right\} \delta + \bar{\beta}_3, \\
\bar{\beta}_2 \geq & \, 2k_s + \delta + \gamma_2, \\
\bar{\beta}_3 \geq & \, 2k_s + \gamma_1 + \left(y_m + \frac{2\lambda\omega_m\alpha_3 x_m}{\xi} \right) \gamma_2,
\end{aligned} \tag{3.45}$$

where $\gamma_1, \gamma_2 > 0$ are bounds on disturbance estimation errors, $k_s > 0$, and v_m, ω_m,$\dot{\omega}_m$, x_m, y_m are defined in Assumptions 1 and 2. Then:

(1) The sliding variable will reach a practical sliding mode;
(2) The posture error will converge to the region $\chi = \{\mathbf{E} \in \Omega_E : \|\mathbf{s}\| \leq \delta\}$.

Proof. Consider the Lyapunov function

$$L = \frac{1}{2}\mathbf{s}^\top\mathbf{s}.$$

Its derivative along sliding variable $\mathbf{s}$ is:

$$\begin{aligned}
\dot{L} = & \, \mathbf{s}^\top \left[\mathbf{F} - \bar{\mathbf{B}}\check{\mathbf{F}} + \mathbf{P}(\mathbf{E}) - \bar{\mathbf{B}}\mathbf{P}(\check{\mathbf{E}}) - \bar{\mathbf{B}}\check{\boldsymbol{\vartheta}} + \mathbf{B}(\mathbf{d} - \check{\hat{\mathbf{d}}}) \right] - \mathbf{s}^\top\bar{\mathbf{B}}\bar{\boldsymbol{\beta}}\text{sign}(\check{\mathbf{s}}) - k\mathbf{s}^\top\bar{\mathbf{B}}\check{\mathbf{s}} \\
\leq & \, |s_1| \Big\{ |v_r| \cos E_\theta - \cos\check{E}_\theta| + |v_r||a(E_y)\sin E_\theta - a(\check{E}_y)\sin\check{E}_\theta| + |\omega_r||b(\check{E}) - b(E)| \\
& + \lambda|\dot{\omega}_r||\Psi(\check{E}_y) - \Psi(E_y)| \Big\} - \mathbf{s}^\top\bar{\mathbf{B}}\check{\boldsymbol{\vartheta}} + \mathbf{s}^\top\mathbf{B}(\mathbf{d} - \check{\hat{\mathbf{d}}}) - \mathbf{s}^\top\bar{\mathbf{B}}\bar{\boldsymbol{\beta}}\text{sign}(\check{\mathbf{s}}) - k\mathbf{s}^\top\bar{\mathbf{B}}\check{\mathbf{s}},
\end{aligned}$$

where

$$\begin{aligned}
\mathbf{F} = & \, \mathbf{J}(\mathbf{E})\mathbf{H}(\mathbf{E}) = \begin{pmatrix} v_r\cos E_\theta + a(E_y)\sin E_\theta \\ \omega_r \end{pmatrix}, \\
\check{\mathbf{F}} = & \, \mathbf{J}(\check{\mathbf{E}})\mathbf{H}(\check{\mathbf{E}}), \\
\bar{\mathbf{B}} = & \, \mathbf{B}(\mathbf{E})\mathbf{B}^{-1}(\check{\mathbf{E}}) = \begin{pmatrix} 1 & b(\check{E}) - b(E) \\ 0 & 1 \end{pmatrix},
\end{aligned}$$

$$\mathbf{P}(\mathbf{E}) - \bar{\mathbf{B}}\mathbf{P}(\check{\mathbf{E}}) = \begin{pmatrix} \lambda\dot{\omega}_r[\Psi(\check{E}_y) - \Psi(E_y)] \\ 0 \end{pmatrix}.$$

With the help of the bounds of $|v_r|$, $|w_r|$, $|\dot{w}_r|$, $|E_y|$, $|E_\theta|$ (see Assumptions 1 and 2), together with the bounds of $|b(\check{E}) - b(E)|$, $|\cos E_\theta - \cos \check{E}_\theta|$, $|a(E_y)\sin E_\theta - a(\check{E}_y)\sin \check{E}_\theta|$, $|\Psi(\check{E}_y) - \Psi(E_y)|$, $\mathbf{s}^{\mathsf{T}}\bar{\mathbf{B}}\check{\boldsymbol{\vartheta}}$, and $\mathbf{s}^{\mathsf{T}}\mathbf{B}(\mathbf{d} - \check{\mathbf{d}})$ (for the detailed derivation, see Appendix A), we can obtain:

$$\begin{aligned} \dot{L} \leq\ & |s_1|\Bigg\{v_m\left(1 + 2\sqrt{1 + (\frac{2\lambda\omega_m\alpha_3}{\xi^2})^2}\right) + (\omega_m + k_s)\left(\frac{\xi^2}{2\lambda\omega_m\alpha_3} + \frac{2\lambda\omega_m\alpha_3}{\xi}(1 + \frac{|\check{E}_x|}{\xi})\right) \\ & + \frac{\xi\dot{\omega}_m}{\omega_m} + \gamma_1 + y_m + \frac{2\lambda\omega_m\alpha_3 x_m}{\xi}\Bigg\}\delta + |s_1|\left[\gamma_1 + \left(y_m + \frac{2\lambda\omega_m\alpha_3 x_m}{\xi}\right)\gamma_2\right] \\ & + |s_2|(\gamma_2 + \delta) + k_s\|\mathbf{s}\| - \mathbf{s}^{\mathsf{T}}\bar{\boldsymbol{\beta}}\mathrm{sign}(\check{\mathbf{s}}) - k\mathbf{s}^{\mathsf{T}}\bar{\mathbf{B}}\check{\mathbf{s}}. \end{aligned} \tag{3.46}$$

Case 1: No sliding variables have reached the sliding surface.

Before the sliding variable $\mathbf{s}$ reaches the sliding surface, the equalities $\mathrm{sign}(\mathbf{s}) = \mathrm{sign}(\check{\mathbf{s}})$ and $b(\check{E}) = b(E)$ hold. Substituting the controller gains specified in (3.45) into (3.46), we derive the following inequality:

$$\begin{aligned} \dot{L} &\leq -2k_s|s_1| - 2k_s|s_2| + k_s\|\boldsymbol{s}\| - k\|\boldsymbol{s}\|^2 \\ &\leq -k_s\|\boldsymbol{s}\| - k\|\boldsymbol{s}\|^2 \leq K_1 L^{1/2} - K_2 L, \end{aligned}$$

where $K_1 = \sqrt{2}k_s$ and $K_2 = 2k$. This inequality ensures the finite-time convergence of the sliding variable $\mathbf{s}$ to the sliding region.

Case 2: All sliding variables lie on the sliding surface.

When all sliding variables satisfy $\|\mathbf{s}\| \leq \delta$, the equality $\mathrm{sign}(\mathbf{s}) = \mathrm{sign}(\check{\mathbf{s}})$ may not hold during triggering intervals $t \in [t_i, t_{i+1}]$. The bound on the sliding variables is derived as follows:

$$\begin{aligned} \|\mathbf{s} - \check{\mathbf{s}}\| &= \left\|\begin{bmatrix} E_x - \lambda\omega_r\Psi(E_y) - \check{E}_x + \lambda\omega_r\Psi(\check{E}_y) \\ E_\theta - \check{E}_\theta \end{bmatrix}\right\| \\ &\leq |E_x - \check{E}_x| + \lambda\omega_m|\Psi(E_y) - \Psi(\check{E}_y)| + |E_\theta - \check{E}_\theta|. \end{aligned} \tag{3.47}$$

Using the Lipschitz continuity of $\Psi(E_y)$ and the event-triggering condition, the following inequality is established:

$$\begin{aligned} \|\mathbf{s}\| \leq \|\mathbf{s} - \check{\mathbf{s}}\| &\leq |E_x - \check{E}_x| + \lambda\omega_m|\Psi(E_y) - \Psi(\check{E}_y)| + |E_\theta - \check{E}_\theta| \\ &\leq |E_x - \check{E}_x| + \frac{2\lambda\omega_m\alpha_3}{\xi}|E_y - \check{E}_y| + |E_\theta - \check{E}_\theta| < \delta. \end{aligned} \tag{3.48}$$

This implies that the sliding variables, once they have reached the sliding surface, will remain within it.

Case 3: Partial sliding variables reach the sliding surface.

Only one sliding variable reaches the sliding surface. Suppose that s_1 attains the sliding surface first, under which condition $\|\mathbf{s}\| > \delta$. If the controller is not in the triggered state, then from Eq (3.47)

together with the triggering condition (3.44), it follows that $\eta(t) \geq \|\mathbf{s} - \check{\mathbf{s}}\| \geq \|\mathbf{s}\| > \delta$, which contradicts the triggering condition. Therefore, the controller is in the triggered state, and according to the result of Case 1, the system state will converge to the sliding surface within finite time. Integrating this result with the conclusion of Case 2 confirms that both sliding variables maintain their sliding motions without escape behavior, thereby completing the proof. □

Remark 9. *Theorem 4 ensures the boundedness of the sliding variable* $\mathbf{s}$*. According to Eqs* (3.1) *and* (3.43)*, we obtain* $|E_\theta| \leq \delta$*. Furthermore, Theorem 3 implies that when the mobile robot's posture errors enter the sliding mode region, they will be attracted to the sliding surface. The posture errors will then move along the sliding surface toward the vicinity of the origin, which guarantees that, under the combined action of controller* (3.42) *and the event-triggering mechanism, the posture error system* (2.4) *will achieve practical stability.*

Remark 10. *In the event-triggered control scheme proposed in [31], the input matrix* $\mathbf{B}_1(\mathbf{e})$ *satisfies*

$$|\mathbf{B}_1(\mathbf{e})| = \lambda + \frac{v_r x_e}{1 + y_e^2},$$

which becomes zero when

$$x_e = -\frac{\lambda(1 + y_e)^2}{v_r},$$

leading to unavoidable singularity problems. To circumvent this issue, authors in [31] requires an appropriately enlarged triggering threshold $\beta(t) \leq \alpha + \gamma^\dagger(x_e, y_e, v_r)$ *when the posture errors approach the region near the singularity point. However, increasing the triggering threshold inevitably degrades the steady-state tracking accuracy. Consequently, Nath's controller cannot achieve high-precision trajectory tracking.*

In contrast, the sliding surface $\mathbf{s}$ *designed in* (3.1) *ensures that the input matrix* $\mathbf{B}(\mathbf{E})$ *inherently avoids singularity issues, as* $|\mathbf{B}(\mathbf{E})| = 1$ *remains constant and independent of the robot's posture tracking errors. This characteristic fundamentally distinguishes our method from that in [31] and eliminates the need for an artificially enlarged triggering threshold to prevent singularity. As a result, our approach achieves a favorable balance between communication resource savings and steady-state error control.*

The event-triggered sliding mode control scheme has been successfully designed, ensuring stability of the mobile robot's posture tracking error system. We now proceed to demonstrate the exclusion of Zeno behavior in the resulting closed-loop system.

Theorem 5. *For the posture tracking error system* (2.4) *with event-triggering condition* $\eta \leq \delta$*, under Assumptions 1-2, the lower bound of triggering intervals* $\Delta T = t_{k+1} - t_k$ *satisfies:*

$$\Delta T \geq \frac{\delta}{\Gamma} \tag{3.49}$$

Proof. Considering the event condition $\eta \leq \delta$ and the fact that $\eta(t_k^+) = 0$, the lower bound of triggering intervals can be derived as:

$$\begin{aligned} \eta(t_{k+1}) - \eta(t_k^+) &\leq \int_{t_k}^{t_{k+1}} \sup\left(|\dot{E}_x| + \frac{2\lambda\alpha_3}{\xi^2}|\dot{E}y| + |\dot{E}\theta| + |\dot{\hat{d}}_1| + |\dot{\hat{d}}_2|\right) d\tau, \\ \delta &\leq \sup\left(|\dot{E}_x| + \frac{2\lambda\alpha_3}{\xi^2}|\dot{E}y| + |\dot{E}\theta| + |\dot{\hat{d}}_1| + |\dot{\hat{d}}_2|\right)\Delta T. \end{aligned} \tag{3.50}$$

Based on Assumption 2 and the convergence properties of the disturbance estimation, it can be concluded that

$$\Gamma \geq \sup\left(|\dot{E}_x| + \frac{2\lambda\alpha_3}{\xi^2}|\dot{E}_y| + |\dot{E}_\theta| + |\dot{\hat{d}}_1| + |\dot{\hat{d}}_2|\right) \tag{3.51}$$

is a bounded positive constant. Substituting this into above equation, the inter-event time satisfies $\Delta T \geq \frac{\delta}{\Gamma}$, which proves the absence of Zeno behavior. □

Remark 11. *In the proposed controller, multiple parameters are involved. Here, the parameter tuning procedure is illustrated. The parameters k, β_1, β_2, λ, and α_3 affect the convergence rate of the system states. Increasing these values shortens the time required to reach the equilibrium point, but simultaneously amplifies the control input. Therefore, these parameters should be chosen judiciously to avoid actuator saturation. Parameter ξ affects the convergence accuracy of sliding mode control and the effective range of the transition function $f_1(x)$; reducing ξ decreases the steady-state error of the robot, but an extremely small ξ may cause oscillation issues. The magnitude of the triggering threshold δ affects the number of actuator triggering events and the actual steady-state tracking error of the robot. A larger δ reduces the communication frequency, but at the cost of increasing the steady-state tracking error. Consequently, parameter selection should strike a balance between communication resource conservation and steady-state error reduction.*

4. Simulation results

To validate the effectiveness of the proposed control scheme, comparative simulations are conducted in the MATLAB/Simulink environment. First, the proposed disturbance observer based sliding mode control scheme is compared with existing control methods, including the finite time sliding mode control (FSMC) approach from [26] combined with the finite time disturbance observer from [22], and the robust siding mode controller from [33] integrated with the fixed-time disturbance observer from [20]. Second, in Experiment 2, the proposed event-triggered control scheme is compared with that in [31] to demonstrate the superiority of the proposed event-triggered sliding mode control scheme.

Simulations are performed in the MATLAB/Simulink environment with a fixed step size of 0.01 s and a total duration of 60 s. The reference trajectory is defined as a circular path characterized by the following equations:

$$\begin{aligned}\dot{x}_r &= v_r\cos(\theta_r),\\ \dot{y}_r &= v_r\sin(\theta_r),\\ \dot{\theta}_r &= \omega_r,\end{aligned}$$

where $v_r = 0.7$ m/s represents the reference linear velocity and $\omega_r = 0.6$ rad/s denotes the reference angular velocity. The initial reference posture is set as $\mathbf{q}_r(0) = [0, 0, 0]^{\mathrm{T}}$.

4.1. Experiment 1

Experiment 1 compares the proposed control scheme with two existing control approaches: a FSMC [26] combined with a disturbance observer (Do1) [23], and a finite-time control (FC) scheme [35] integrated with a fixed-time disturbance observer (Do2) [19].

(1) FSMC [26]:

$$S = \xi_1 + k_1 \int \text{sign}(\xi_1) d\tau, \tag{4.1}$$

where

$$\xi_1 = \begin{bmatrix} E_x \\ E_\theta + \frac{\rho}{|E_x|+\rho} \tan^{-1} E_y \end{bmatrix}, \tag{4.2}$$

$$V_c = (HG)^{-1}(-k_2 \text{sign}(s) - \Phi) - \hat{\delta}, \tag{4.3}$$

where

$$\begin{aligned} HG &= \begin{bmatrix} -1 & 0 \\ \frac{\rho \text{sign}(E_x))}{(|E_x|+\rho)^2} \tan^{-1}(E_y) & -1 \end{bmatrix}, \quad H = \begin{bmatrix} 1 & 0 & 0 \\ -\frac{\rho \text{sign}(E_x))}{(|E_x|+\rho)^2} \tan^{-1}(E_y) & \frac{\rho}{(|E_x|+\rho)(1+E_y^2)} & 1 \end{bmatrix}, \\ F &= \begin{bmatrix} \omega y_e + v_r \cos(\phi_e) \\ -\omega x_e + v_r \sin(\phi_e) \\ \omega_r \end{bmatrix}, \quad \Phi = HF + k_1 \text{sign}(\xi_1), \end{aligned} \tag{4.4}$$

with controller gains $k_1 = k_2 = 1$.

(2) FC [35]:

$$V_c = \Phi_1^+(R(-k\text{sig}(e)^\gamma - \Phi_3 e) - \Phi_2) - \hat{\delta}, \tag{4.5}$$

where

$$\begin{aligned} \Phi_1^+ &= \begin{bmatrix} -1 & 0 & 0 \\ 0 & 0 & -1 \end{bmatrix}, \quad R = \begin{bmatrix} \cos\theta & \sin\theta & 0 \\ -\sin\theta & \cos\theta & 0 \\ 0 & 0 & 1 \end{bmatrix}, \\ \Phi_2 &= \begin{bmatrix} \omega y_e + v_r \cos(\phi_e) \\ -\omega x_e + v_r \sin(\phi_e) \\ \omega_r \end{bmatrix}, \quad \Phi_3 = \begin{bmatrix} 0 & -\omega & 0 \\ \omega & 0 & 0 \\ 0 & 0 & 0 \end{bmatrix}, \end{aligned} \tag{4.6}$$

with controller gains $k = 1$, $\gamma = 0.5$.

(3) Proposed controller: The control law is given by (3.29), with the disturbance observer (3.6) and adaptive mechanism (3.23). The controller and adaptive disturbance observer parameters are listed in Table 1.

Table 1. Controller Parameters of proposed controller.

Method	Parameters
sliding surface	$k_1 = 0.5, \xi = 0.5, \lambda = 1, \alpha_3 = 1$
Controller	$\beta = \begin{bmatrix} 3 & 0 \\ 0 & 3 \end{bmatrix}, k = 1, k_s = 2, \lambda_s = 0.05$
Disturbance observer	$\kappa_1 = \begin{bmatrix} 2 & 0 \\ 0 & 2 \end{bmatrix}, \kappa_2 = \begin{bmatrix} 2 & 0 \\ 0 & 2 \end{bmatrix}$
Adaptive mechanism	$\mu_{1i} = 10, r_{0i} = 0.1, \mu_{2i} = 10, \mu_{3i} = 0.1, \varepsilon_i = 0.1$

Experiment 1 consists of two cases with different initial conditions and disturbances. In Case 1, the initial posture of the robot is $\mathbf{p}(0) = (-1, -1, 0)^{\mathsf{T}}$, and the unknown disturbance is given by

$$\mathbf{d}(t) = \begin{bmatrix} 0.2\sin(0.5t) \\ 0.2\sin(t) + 0.3\cos(0.5t) \end{bmatrix}. \tag{4.7}$$

In Case 2, the initial posture of the robot is $\mathbf{p}(0) = (-1.5, -2, \pi/4)^{\mathsf{T}}$, and the unknown disturbance is given by

$$\mathbf{d}(t) = \begin{bmatrix} 0.5 \\ 0.4\sin(0.3t) + 0.2 \end{bmatrix}. \tag{4.8}$$

Remark 12. *The cumulative control energy consumption is defined as*

$$E_u(t) = \int_0^t \|\mathbf{V}_c(\tau)\| d\tau, \tag{4.9}$$

where $\mathbf{V}_c$ *denotes the control input vector.*

The simulation results are presented in Figures 4–13. Figures 4–7 illustrate the trajectory tracking curves and the corresponding tracking errors of the robot. From Tables 2 and 3, it can be observed that the proposed control scheme achieves convergence times of 7.94 s and 8.13 s in the E_x direction, respectively, which are faster than those of FSMC and FC. In terms of E_x and E_y, the proposed method yields the smallest maximum steady-state error (MAX) and integral of absolute error (IAE), although it does not exhibit an advantage in E_θ.The responses of the sliding variables and the control inputs are shown in Figures 8–11. As can be seen from the zoomed-in views, the FSMC scheme suffers from chattering, whereas the proposed controller exhibits significantly reduced oscillations. Moreover, in terms of energy consumption, the proposed scheme achieves the lowest values of 29.79 and 33.32, respectively. Figures 12 and 13 present the disturbance estimation error curves of the observers. It is evident that the proposed controller achieves higher estimation accuracy, while Do1 suffers from chattering issues.

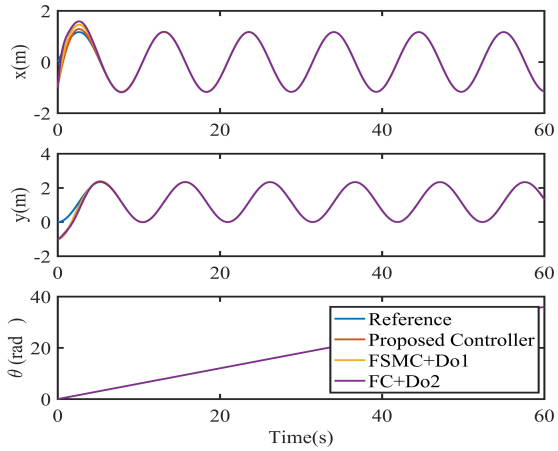

Figure 4. Robot position in Case 1.

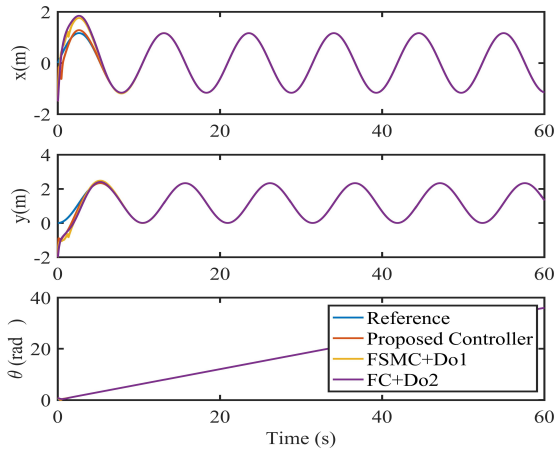

Figure 5. Robot position in Case 2.

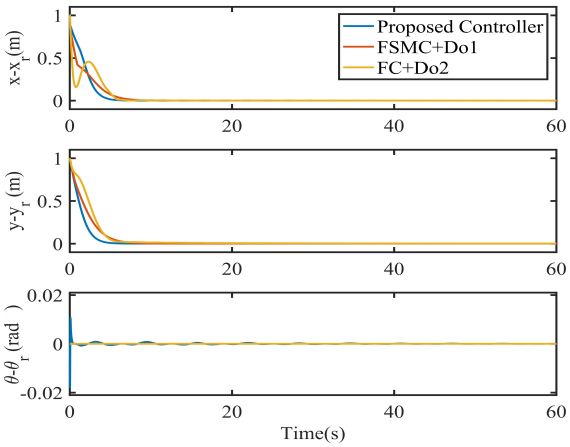

Figure 6. Posture tracking error in Case 1.

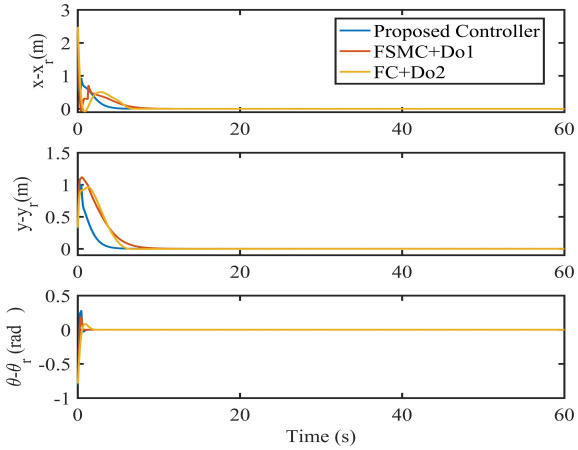

Figure 7. Posture tracking error in Case 2.

Table 2. Tracking performance of different controllers in Case 1.

Tracking errors	Controller	IAE	MAX	Setting time	Energy
E_x	Proposed controller	1.665 m	1.1×10^{-4}m	7.94 s	29.79
	FSMC+Do1	1.675 m	3.4×10^{-3} m	8.42 s	57.51
	FC+Do2	1.719 m	2.1×10^{-3} m	9.61 s	57.62
E_y	Proposed controller	1.339 m	1.2×10^{-4} m	7.78 s	
	FSMC+Do1	2.603 m	4.6×10^{-3} m	10.18 s	
	FC+Do2	1.972 m	5.2×10^{-3}m	10.87 s	
E_θ	Proposed controller	0.142 rad	2.5×10^{-3}rad	4.67 s	
	FSMC+Do1	0.004 rad	2.4×10^{-4}rad	1.24 s	
	FC+Do2	0.002 rad	5.2×10^{-3}rad	1.56 s	

Table 3. Tracking performance of different controllers in Case 2.

Tracking errors	Controller	IAE	MAX	Setting time	Energy
E_x	Proposed controller	1.647 m	1.2×10^{-4}m	8.13 s	33.32
	FSMC+Do1	2.913 m	6.5×10^{-3} m	9.32 s	59.68
	FC+Do2	2.198 m	4.5×10^{-3} m	10.24 s	59.82
E_y	Proposed controller	1.306 m	1.1×10^{-4} m	7.86 s	
	FSMC+Do1	3.238 m	2.4×10^{-3} m	10.18 s	
	FC+Do2	3.426 m	3.2×10^{-3}m	12.04 s	
E_θ	Proposed controller	0.217 rad	3.1×10^{-4}rad	1.93 s	
	FSMC+Do1	0.229 rad	2.4×10^{-4}rad	2.23 s	
	FC+Do2	0.198 rad	2.1×10^{-3}rad	3.51 s	

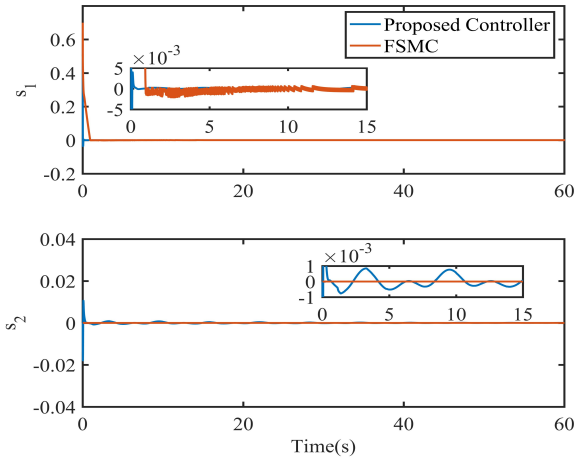

Figure 8. Sliding variable in Case 1.

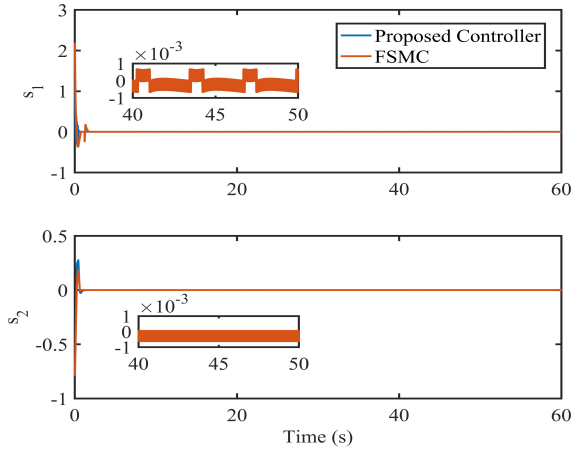

Figure 9. Sliding variable in Case 2.

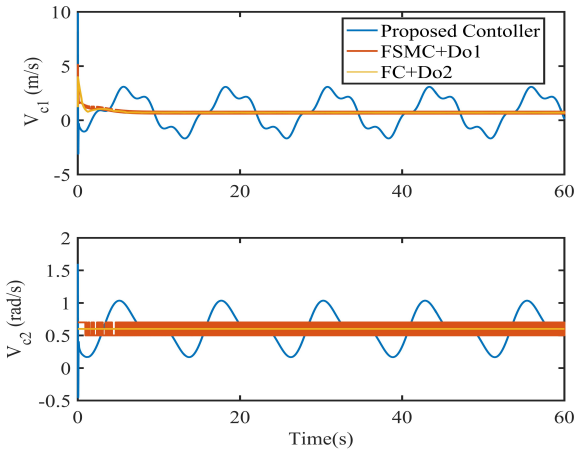

Figure 10. Control input in Case 1.

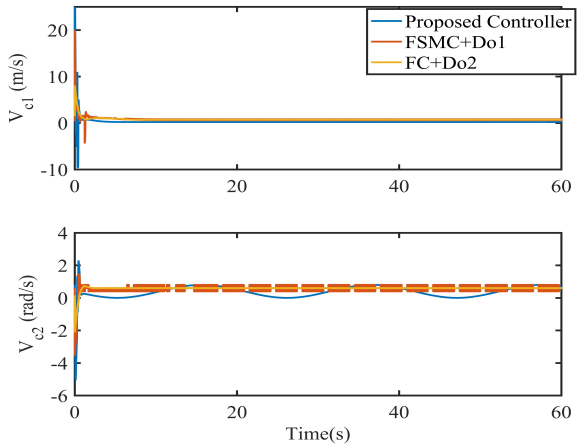

Figure 11. Control input in Case 2.

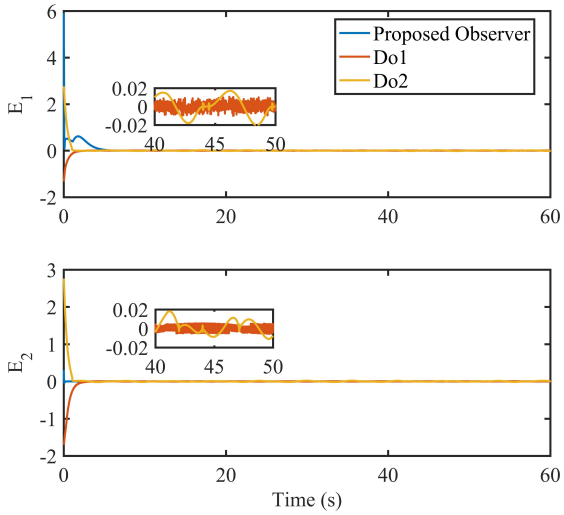

Figure 12. Disturbance estimation error in Case 1.

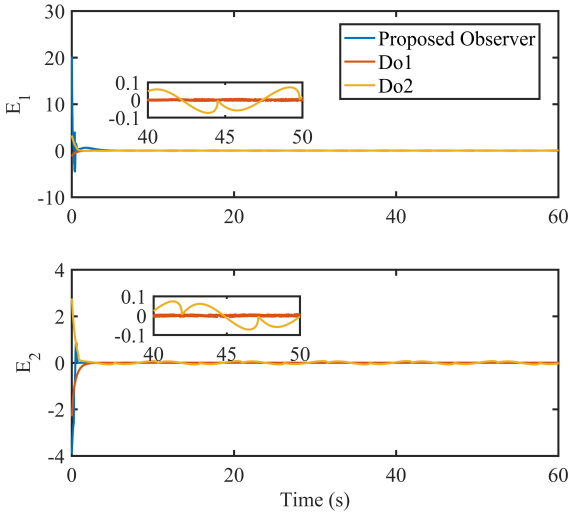

Figure 13. Disturbance estimation error in Case 2.

Based on the above results, it can be concluded that the proposed control scheme is more robust and faster in terms of disturbance rejection capability and settling-time convergence.

4.2. Experiment 2

In experiment 2, we conduct numerical simulations to validate the proposed event-triggered sliding mode control scheme. The reference trajectory and external disturbance conditions remain identical to those in Case 1, with the maximum reference linear velocity $v_{\max} = 0.7$ and maximum reference angular velocity $\omega_{\max} = 0.6$. The finite-time sliding surface parameters are configured as $\xi = 0.5$, $\lambda = 1$, and $k_1 = 0.5$. The event-triggering threshold is selected as $\delta = 0.02$, while the parameters for the disturbance observer, adaptive mechanism, and saturation function maintain the same settings

as Case 1 in Experiment 1. The controller gains must satisfy the conditions specified in Eq (3.45), yielding the following values based on the relevant parameters:

$$\bar{\beta}_1 = |E_x(t)| + \bar{\beta}_3, \quad \bar{\beta}_2 = 2, \quad \text{and} \quad \bar{\beta}_3 = 3.$$

The controller parameters in [33] are selected as follows:

$$\lambda = 1, \quad \rho = 0.05, \quad \varpi = 0.5, \quad c_1 = c_2 = c_3 = 1, \quad d_m = 1, \quad v_m = w_m = 1.$$

All simulations employ a fixed step size of 0.002 seconds.

Figures 14–19 illustrate the experimental results. From Figures 14 and 15, it is evident that due to the large triggering threshold required by the controller in [33] to avoid the singularity problem, its steady-state tracking accuracy is degraded. The maximum absolute errors of that controller for E_x, E_y, and E_θ are 0.031, 0.072, and 0.081, respectively, and all higher than those of the proposed controller (0.005, 0.017, and 0.008). Figures 16 and 17 present the sliding variable trajectories and control inputs, respectively. The maximum control inputs of the proposed controller are 4 m/s and 0.15 rad/s, both smaller than those of Nath's controller. Figures 18 and 19 show the inter-event intervals and the number of triggering events. The proposed controller achieves a maximum inter-event interval of 0.57 s, whereas Nath's controller attains 1.62 s. Over a simulation horizon of 60 s, the two schemes are triggered 362 and 124 times, respectively. These results indicate that although Nath's controller offers a lower triggering frequency, the proposed controller provides higher tracking accuracy, achieving a favorable balance between triggering efficiency and tracking performance. Moreover, Case 1 in Experiment 1 corresponds to the scenario without an event-triggering mechanism, where the communication count reaches 35,000. Consequently, while the proposed event-triggered control scheme reduces communication resource consumption compared with the continuous control method, it inevitably leads to an increased steady-state error.

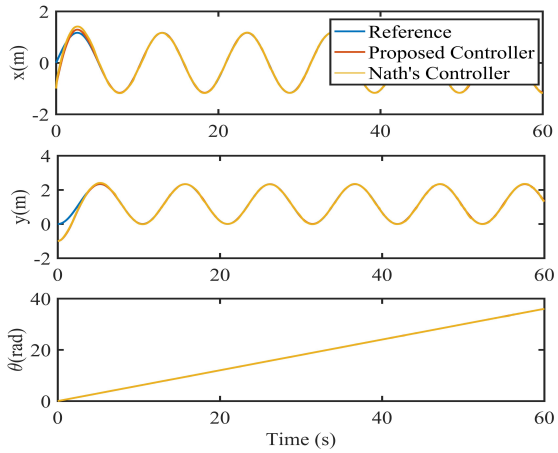

Figure 14. Robot position.

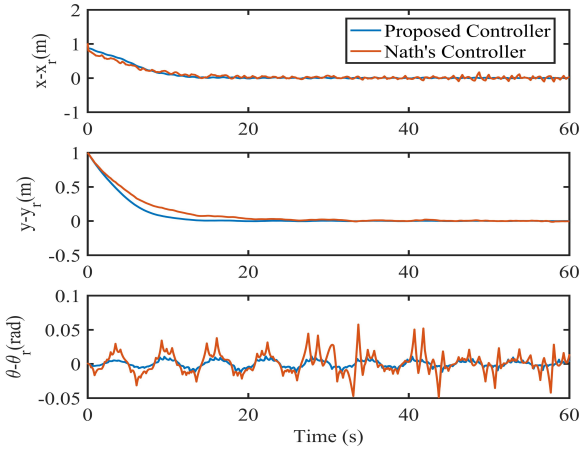

Figure 15. Robot posture tracking error.

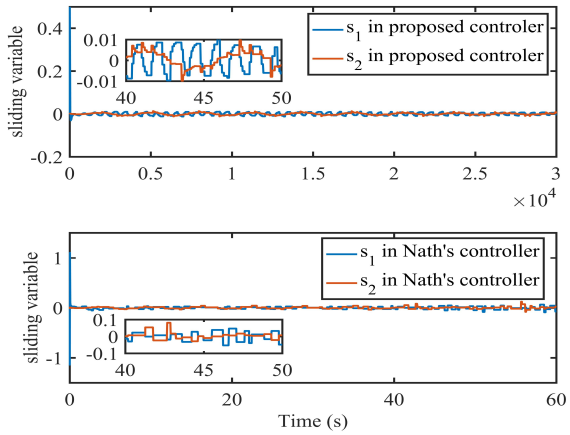

Figure 16. Sliding variable.

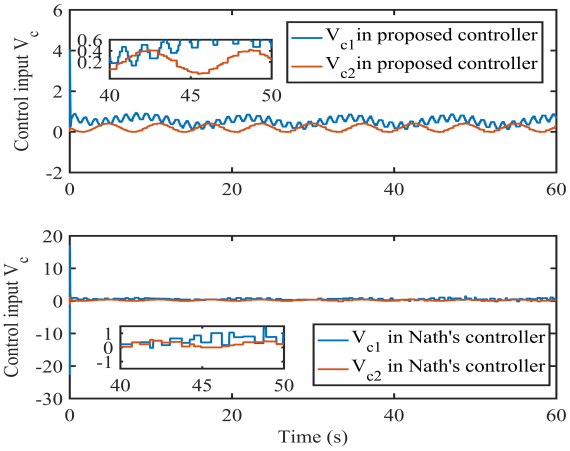

Figure 17. Control input.

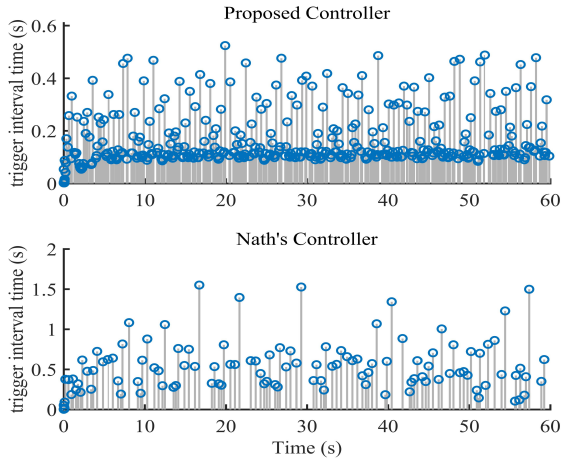

Figure 18. Time between two triggering executions.

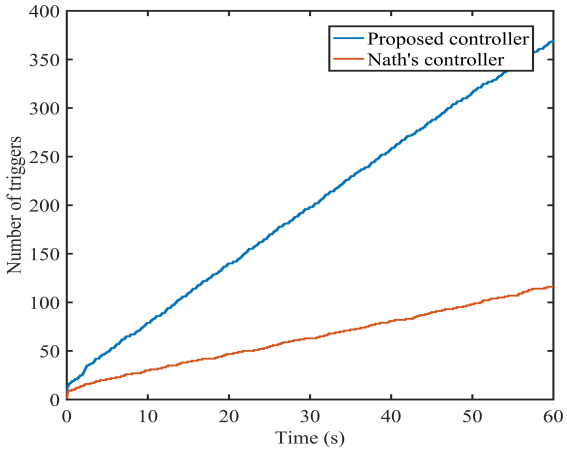

Figure 19. Triggered times.

5. Conclusions

In this paper, we propose an event-triggered sliding mode control scheme for trajectory tracking of differential-drive mobile robots under unknown disturbances and limited communication resources. A novel piecewise sliding surface is constructed to eliminate the singularity problem and guarantee predefined steady-state tracking accuracy. An adaptive disturbance observer is designed to achieve chattering-free estimation without requiring prior knowledge of disturbance bounds. Furthermore, an event-triggered mechanism integrated with the sliding mode controller avoids the high-gain issue and reduces communication resource consumption. The practical stability of the closed-loop error dynamics has been rigorously established via Lyapunov methods, and comparative MATLAB simulations have demonstrated faster convergence, smaller steady-state errors, and a favorable balance between tracking precision and communication efficiency.

Nevertheless, two limitations of the proposed scheme should be acknowledged. The controller involves a relatively large number of parameters, which may complicate practical tuning. Moreover,

actuator faults are not considered in the current design, limiting its applicability in fault-prone scenarios. These limitations naturally define future research directions: reducing the number of controller parameters and extending the proposed framework to handle actuator faults, thereby further enhancing its practicality and robustness.

Author contributions

Z. Chen: writing-original draft, software, methodology; D. Liao: writing-original draft, software, methodology; W. Yang: writing-review & editing, resources, investigation; Y. Alexander: validation, writing-review & editing, supervision. All authors have read and agreed to the published version of the manuscript.

Use of Generative-AI tools declaration

The authors declare they have used Artificial Intelligence (AI) tools in the creation of this article. DeepSeek was utilized to revise and improve the content, particularly in the "Introduction" section, by enhancing language expression and logical structure.

Conflict of interest

All authors declare no conflicts of interest in this paper.

References

1. I. U. Rehman, A. Abadi, M. Labbadi, L. L. Y. Voon, Safety and control of wheeled mobile robots using differential flatness under disturbances, *Seventeenth International Conference on Quality Control by Artificial Vision*, **13737** (2025), 143–150. https://doi.org/10.1117/12.3001234
2. W. Yuan, Y. Liu, Y. H. Liu, C. Y. Su, Differential flatness-based adaptive robust tracking control for wheeled mobile robots with slippage disturbances, *ISA Trans.*, **144** (2024), 482–489. https://doi.org/10.1016/j.isatra.2023.11.005
3. H. Ebel, M. Rosenfelder, P. Eberhard, Cooperative object transportation with differential-drive mobile robots: control and experimentation, *Robot. Auton. Syst.*, **173** (2024), 104612. https://doi.org/10.1016/j.robot.2023.104612
4. T. Fukao, H. Nakagawa, N. Adachi, Adaptive tracking control of a nonholonomic mobile robot, *IEEE Trans. Robot. Autom.*, **16** (2000), 609–615. https://doi.org/10.1109/70.880812
5. Q. Lu, J. Chen, Q. Wang, D. Zhang, M. Sun, C. Y. Su, Practical fixed-time trajectory tracking control of constrained wheeled mobile robots with kinematic disturbances, *ISA Trans.*, **129** (2022), 273–286. https://doi.org/10.1016/j.isatra.2022.02.005
6. J. Tang, S. Wu, B. Lan, Y. Dong, Y. Jin, G. Tian, et al., GMPC: geometric model predictive control for wheeled mobile robot trajectory tracking, *IEEE Robot. Autom. Lett.*, **9** (2024), 4822–4829. https://doi.org/10.1109/LRA.2024.3381088

7. J. Yu, Z. Zhu, J. Lu, S. Yin, Y. Zhang, Modeling and MPC-based pose tracking for wheeled bipedal robot, *IEEE Robot. Autom. Lett.*, **8** (2023), 7881–7888. https://doi.org/10.1109/LRA.2023.3325628
8. J. A. Rodríguez-Arellano, R. Miranda-Colorado, L. T. Aguilar, M. A. Negrete-Villanueva, Trajectory tracking nonlinear H∞ controller for wheeled mobile robots with disturbances observer, *ISA Trans.*, **142** (2023), 372–385. https://doi.org/10.1016/j.isatra.2023.07.037
9. R. Miranda-Colorado, Observer-based finite-time control for trajectory tracking of wheeled mobile robots with kinematic disturbances, *ISA Trans.*, **148** (2024), 64–77. https://doi.org/10.1016/j.isatra.2024.03.031
10. L. Wu, J. Liu, S. Vazquez, S. K. Mazumder, Sliding mode control in power converters and drives: a review, *IEEE/CAA J. Autom. Sin.*, **9** (2021), 392–406. https://doi.org/10.1109/JAS.2021.1004380
11. M. Labbadi, M. Cherkaoui, Robust adaptive nonsingular fast terminal sliding-mode tracking control for an uncertain quadrotor UAV subjected to disturbances, *ISA Trans.*, **99** (2020), 290–304. https://doi.org/10.1016/j.isatra.2019.10.012
12. M. Gao, X. Jin, L. Ding, A novel nonsingular fixed-time sliding mode control of uncertain Euler–Lagrange systems, *IEEE Syst. J.*, **17** (2022), 467–478. https://doi.org/10.1109/JSYST.2022.3211521
13. M. Ghasemi, S. G. Nersesov, G. Clayton, Finite-time tracking using sliding mode control, *J. Franklin Inst.*, **351** (2014), 2966–2990. https://doi.org/10.1016/j.jfranklin.2014.01.018
14. B. Moudoud, H. Aissaoui, M. Diany, Finite-time adaptive trajectory tracking control based on sliding mode for wheeled mobile robot, *2021 18th International Multi-Conference on Systems, Signals & Devices (SSD)*, 2021, 1148–1153. https://doi.org/10.1109/SSD52085.2021.9429380
15. J. M. Yang, J. H. Kim, Sliding mode control for trajectory tracking of nonholonomic wheeled mobile robots, *IEEE Trans. Robot. Autom.*, **15** (1999), 578–587. https://doi.org/10.1109/70.768190
16. D. Chwa, Sliding-mode tracking control of nonholonomic wheeled mobile robots in polar coordinates, *IEEE Trans. Control Syst. Technol.*, **12** (2004), 637–644. https://doi.org/10.1109/TCST.2004.824953
17. M. Van, S. S. Ge, Adaptive fuzzy integral sliding-mode control for robust fault-tolerant control of robot manipulators with disturbance observer, *IEEE Trans. Fuzzy Syst.*, **29** (2020), 1284–1296. https://doi.org/10.1109/TFUZZ.2020.2973955
18. Z. Yu, Y. Qu, Y. Zhang, Distributed fault-tolerant cooperative control for multi-UAVs under actuator fault and input saturation, *IEEE Trans. Control Syst. Technol.*, **27** (2018), 2417–2429. https://doi.org/10.1109/TCST.2018.2868038
19. W. Liu, M. Chen, P. Shi, Fixed-time disturbance observer-based control for quadcopter suspension transportation system, *IEEE Trans. Circuits Syst. I*, **69** (2022), 4632–4642. https://doi.org/10.1109/TCSI.2022.3193878
20. B. Li, H. Liu, C. K. Ahn, C. Wang, X. Zhu, Fixed-time tracking control of wheel mobile robot in slipping and skidding conditions, *IEEE/ASME Trans. Mechatron.*, **30** (2024), 1865–1875. https://doi.org/10.1109/TMECH.2024.3401069

21. D. Shi, J. Zhang, Z. Sun, G. Shen, Y. Xia, Composite trajectory tracking control for robot manipulator with active disturbance rejection, *Control Eng. Pract.*, **106** (2021), 104670. https://doi.org/10.1016/j.conengprac.2020.104670

22. Y. Fei, P. Shi, C. P. Lim, X. Yuan, Finite-time observer-based formation tracking with application to omnidirectional robots, *IEEE Trans. Ind. Electron.*, **70** (2022), 10598–10606. https://doi.org/10.1109/TIE.2022.3224186

23. K. Wu, J. Hu, Z. Ding, F. Arvin, Finite-time fault-tolerant formation control for distributed multi-vehicle networks with bearing measurements, *IEEE Trans. Autom. Sci. Eng.*, **21** (2023), 1346–1357. https://doi.org/10.1109/TASE.2023.3239748

24. V. C. Nguyen, M. T. Vu, S. H. Kim, A finite-time non-singular fast terminal sliding mode control of wheeled mobile robots with prescribed performance, *IET Control Theory Appl.*, **19** (2025), e70013. https://doi.org/10.1049/cth2.70013

25. J. Huang, M. Zhang, S. Ri, C. Xiong, Z. Li, Y. Kang, High-order disturbance-observer-based sliding mode control for mobile wheeled inverted pendulum systems, *IEEE Trans. Ind. Electron.*, **67** (2019), 2030–2041. https://doi.org/10.1109/TIE.2019.2903778

26. H. Xie, J. Zheng, Z. Sun, H. Wang, R. Chai, Finite-time tracking control for nonholonomic wheeled mobile robot using adaptive fast nonsingular terminal sliding mode, *Nonlinear Dyn.*, **110** (2022), 1437–1453. https://doi.org/10.1007/s11071-022-07682-2

27. Z. Li, J. Zhai, Super-twisting sliding mode trajectory tracking adaptive control of wheeled mobile robots with disturbance observer, *Int. J. Robust Nonlinear Control*, **32** (2022), 9869–9881. https://doi.org/10.1002/rnc.6343

28. Y. Guan, T. Shi, J. Zhang, L. Jin, Edge-based event-triggered control for collaborative robot systems, *IEEE Trans. Ind. Electron.*, **73** (2026), 1–11. https://doi.org/10.1109/TIE.2026.3657010

29. C. H. Zhang, L. H. Zhang, L. Wang, Y. Zhang, W. Ding, et al., Dynamic event-triggered control for flexible joint robot based on fully actuated system approach, *IEEE Trans. Cybern.*, **55** (2025), 1738–1746. https://doi.org/10.1109/TCYB.2025.3630202

30. S. Wan, Y. Zhang, Z. He, L. Chen, Periodic event-triggered tracking control for nonholonomic wheeled mobile robots, *Int. J. Innov. Comput. Inf. Control*, **18** (2022), 1507–1517. https://doi.org/10.24507/ijicic.18.05.1507

31. Y. Yan, S. Yu, X. Gao, D. Wu, T. Li, Continuous and periodic event-triggered sliding-mode control for path following of underactuated surface vehicles, *IEEE Trans. Cybern.*, **54** (2024), 449–461. https://doi.org/10.1109/TCYB.2023.3265039

32. W. Qiu, J. Cai, J. He, Synchronization between two non-autonomous chaotic systems via intermittent event-triggered control, *Int. J. Innov. Comput. Inf. Control*, **19** (2023), 907–926. https://doi.org/10.24507/ijicic.19.03.907

33. K. Nath, A. Yesmin, A. Nanda, M. K. Bera, Event-triggered sliding-mode control of two wheeled mobile robot: An experimental validation, *IEEE J. Emerg. Sel. Top. Ind. Electron.*, **2** (2021), 218–226. https://doi.org/10.1109/JESTIE.2021.3087965

34. Y. Shen, X. Xia, Semi-global finite-time observers for nonlinear systems, *Automatica*, **44** (2008), 3152–3156. https://doi.org/10.1016/j.automatica.2008.05.015

35. Y. Wu, Y. Wang, H. Fang, Full-state constrained neural control and learning for the nonholonomic wheeled mobile robot with unknown dynamics, *ISA Trans.*, **125** (2022), 22–30. https://doi.org/10.1016/j.isatra.2021.06.012

Appendix

Boundedness of b: According to Eq (3.4) together with Assumptions 1 and 2, we have

$$|b| \leq |E_y| + \lambda|\omega_r||E_x||\Pi(E_y)| \leq y_m + \lambda\omega_m x_m|\Pi(y_m)|. \tag{A.1}$$

This implies that b is bounded.

Bounds and Lipschitz constant of $\Pi(y)$: Consider the piecewise function given by

$$\Pi(y) = \begin{cases} -2\left(\frac{\alpha_2}{\xi^2} + \alpha_5\right)|y| + \alpha_2\left(\frac{2}{\xi} + 1\right) + \alpha_4\alpha_5, & |y| < \xi, \\ \alpha_1 \sin(2|y|) + \alpha_2, & \xi \leq |y| < 1, \\ \frac{2}{3}\alpha_3|y|^{-\frac{1}{3}}, & |y| \geq 1, \end{cases} \tag{A.2}$$

where $\alpha_3 > 0$, $0 < \xi < 1$, and

$$\begin{aligned} &\alpha_1 = \frac{\alpha_3}{6\sin 2 - 3\sin^2 1} \approx 0.30\alpha_3, \quad \alpha_2 = \frac{3\sin 2 - 2\sin^2 1}{6\sin 2 - 3\sin^2 1}\alpha_3 \approx 0.39\alpha_3, \\ &\alpha_4 = \frac{2\sin^2\xi - \xi\sin(2\xi)}{\sin^2\xi - \xi\sin(2\xi)}\xi, \qquad \alpha_5 = \frac{\sin^2\xi - \xi\sin(2\xi)}{\xi^2}\alpha_1. \end{aligned} \tag{A.3}$$

Its derivative with respect to y is

$$\dot{\Pi}(y) = \text{sign}(y)\begin{cases} -2\left(\frac{\alpha_2}{\xi^2} + \alpha_5\right), & |y| < \xi, \\ 2\alpha_1\cos(2|y|), & \xi \leq |y| < 1, \\ -\frac{2}{9}\alpha_3|y|^{-\frac{4}{3}}, & |y| \geq 1. \end{cases} \tag{A.4}$$

Then the bounds of $\Pi(y)$ and $\dot{\Pi}(y)$ are: For $|y| < \xi$, and note that the function $\Pi(y)$ is continuous, so we can obtain:

$$\begin{aligned} &|\Pi(y)| \leq \alpha_1|\sin(2|\xi|)| + \alpha_2 \leq \alpha_1 + \alpha_2 \leq \frac{2\alpha_3}{\xi}, \\ &|\dot{\Pi}(y)| = 2\left|\frac{\alpha_2}{\xi^2} + \alpha_5\right| \leq 2(\frac{\alpha_2}{\xi^2} + \frac{\alpha_1}{\xi^2}) \leq \frac{2\alpha_3}{\xi^2}. \end{aligned}$$

For $\xi \leq |y| < 1$:

$$|\Pi(y)| \leq \alpha_1 + \alpha_2 < \alpha_3, \quad |\dot{\Pi}(y)| < 2\alpha_1 < \alpha_3.$$

For $|y| \geq 1$:

$$|\Pi(y)| \leq \frac{2}{3}\alpha_3, \quad |\dot{\Pi}(y)| \leq \alpha_3.$$

Thus, we conclude:

$$\sup|\Pi(y)| = \frac{2\alpha_3}{\xi}, \quad L_\Pi = \sup|\dot{\Pi}(y)| = \frac{2\alpha_3}{\xi^2}. \tag{A.5}$$

The bound of $|\Psi(E_y) - \Psi(\check{E}_y)|$:

According to the Lipschitz condition and trigger condition, we can directly obtain

$$|\Psi(E_y) - \Psi(\check{E}_y)| \leq \frac{2\alpha_3}{\xi}|E_y - \check{E}_y| \leq \frac{\xi\delta}{\lambda\omega_m}. \tag{A.6}$$

The bound of $|a(E_y) - a(\check{E}_y)|$:

Based on (3.4), define the function:

$$f_a(E_y) = -\lambda\omega_r\Pi(E_y). \tag{A.7}$$

Taking the partial derivative of $f_a(E_y)$ with respect to E_y, we obtain:

$$\left|\frac{\partial f_a}{\partial E_y}\right| = \lambda|\omega_r|\left|\dot{\Pi}(E_y)\right| \leq \frac{2\lambda\omega_m\alpha_3}{\xi^2}. \tag{A.8}$$

Hence, the Lipschitz constant of $f_z(E_y)$ can be expressed as:

$$L_a \triangleq \sup\left|\frac{\partial f_a}{\partial E_y}\right| = \frac{2\lambda\omega_m\alpha_3}{\xi^2}. \tag{A.9}$$

Then, based on the trigger condition and the Lipschitz constant of $f_z(E_y)$, it can be readily derived that:

$$|a(E_y) - a(\check{E}_y)| \leq L_a|E_y - \check{E}_y| \leq \delta. \tag{A.10}$$

Bound of $|b(E) - b(\check{E})|$:

From (3.4), (3.43) and trigger condition, the following bound can be derived:

$$\begin{aligned}
|b(E) - b(\check{E})| &\leq |E_y - \check{E}_y| + \lambda\omega_m\left|E_x\Pi(E_y) - \check{E}_x\Pi(\check{E}_y)\right| \\
&\leq |E_y - \check{E}_y| + \lambda\omega_m\left(|\Pi(E_y)||E_x - \check{E}_x| + |\check{E}_x||\Pi(E_y) - \Pi(\check{E}_y)|\right) \\
&\leq |E_y - \check{E}_y| + \lambda\omega_m\left(|\Pi(E_y)| + |\check{E}_x|L_\Pi\right)|E_x - \check{E}_x| \\
&\leq \left[\frac{\xi^2}{2\lambda\omega_m\alpha_3} + \frac{2\lambda\omega_m\alpha_3}{\xi}(1 + \frac{|\check{E}_x|}{\xi})\right]\delta.
\end{aligned} \tag{A.11}$$

Bound of $|\cos E_\theta - \cos\check{E}_\theta|$:

$$|\cos E_\theta - \cos\check{E}_\theta| \leq |E_\theta - \check{E}_\theta| \leq \delta. \tag{A.12}$$

Bound of $|a(E_y)\sin E_\theta - a(\check{E}_y)\sin\check{E}_\theta|$: Define the bivariate function

$$f(E_y, E_\theta) \triangleq -\lambda\omega_r\Pi(E_y)\sin(E_\theta).$$

The partial derivatives satisfy:

$$\frac{\partial f}{\partial E_y} = -\lambda\omega_r\dot{\Pi}(E_y)\sin(E_\theta), \quad \frac{\partial f}{\partial E_\theta} = -\lambda\omega_r\Pi(E_y)\cos(E_\theta).$$

The gradient norm of $f(E_y, E_\theta)$ is bounded by:

$$\begin{aligned}\|\nabla f\| &= \sqrt{\left(\frac{\partial f}{\partial E_y}\right)^2 + \left(\frac{\partial f}{\partial E_\theta}\right)^2} \leq \lambda\omega_m \sqrt{\dot{\Pi}(E_y)^2 + \Pi(E_y)^2} \\ &\leq \lambda\omega_m \sqrt{(\frac{2\alpha_3}{\xi^2})^2(1+\xi^2)} \leq \frac{4\lambda\omega_m\alpha_3}{\xi^2}.\end{aligned}$$

Thus, we obtain the bound:

$$\begin{aligned}|a(E_y)\sin E_\theta - a(\check{E}_y)\sin \check{E}_\theta| &\leq \sup\|\nabla f\| \sqrt{(E_y-\check{E}_y)^2 + (E_\theta - \check{E}_\theta)^2} \\ &\leq \frac{4\lambda\omega_m\alpha_3\delta}{\xi^2}\sqrt{1+(\frac{\xi^2}{2\lambda\omega_m\alpha_3})^2} \\ &\leq 2\delta\sqrt{1+(\frac{2\lambda\omega_m\alpha_3}{\xi^2})^2}.\end{aligned} \tag{A.13}$$

The bound of $\mathbf{s}^{\mathrm{T}}\bar{\mathbf{B}}\check{\vartheta}$: The term $\mathbf{s}^{\mathrm{T}}\bar{\mathbf{B}}\check{\vartheta}$ can be rewritten as

$$\mathbf{s}^{\mathrm{T}}\bar{\mathbf{B}}\check{\vartheta} = \mathbf{s}^{\mathrm{T}}(\mathbf{I}+\mathbf{B}_1)\check{\vartheta} = \mathbf{s}^{\mathrm{T}}\check{\vartheta} + \mathbf{s}^{\mathrm{T}}\mathbf{B}_1\check{\vartheta},$$

where I is the identity matrix,

$$\mathbf{B}_1 = \begin{pmatrix} 0 & b(\check{E}) - b(E) \\ 0 & 0 \end{pmatrix}.$$

For $\mathbf{s}^{\mathrm{T}}\check{\vartheta}$, based on Cauchy–Schwarz inequality, we can derive:

$$\mathbf{s}^{\mathrm{T}}\check{\vartheta} = \frac{k_s^2\mathbf{s}^{\mathrm{T}}\check{\mathbf{s}}}{k_s\|\check{\mathbf{s}}\| + \exp(-\lambda_s t_k)} \leq \frac{k_s^2\|\mathbf{s}\|\|\check{\mathbf{s}}\|}{k_s\|\check{\mathbf{s}}\|} \leq k_s\|\mathbf{s}\|. \tag{A.14}$$

For $\mathbf{s}^{\mathrm{T}}\mathbf{B}_1\check{\vartheta}$, we obtain:

$$\begin{aligned}\mathbf{s}^{\mathrm{T}}\mathbf{B}_1\check{\vartheta} &= \frac{k_s^2 s_1\check{s}_2(b(\check{E}) - b(E))}{k_s\|\check{\mathbf{s}}\| + \exp(-\lambda_s t_k)} \\ &\leq \frac{k_s^2|s_1|\|\check{\mathbf{s}}\||b(\check{E}) - b(E)|}{k_s\|\check{\mathbf{s}}\|} \\ &\leq k_s|s_1|\left[\frac{\xi^2}{2\lambda\omega_m\alpha_3} + \frac{2\lambda\omega_m\alpha_3}{\xi}(1+\frac{|\check{E}_x|}{\xi})\right]\delta.\end{aligned} \tag{A.15}$$

Therefore, the boundary value is:

$$\mathbf{s}^{\mathrm{T}}\bar{\mathbf{B}}\check{\vartheta} \leq k_s\|\mathbf{s}\| + k_s|s_1|\left[\frac{\xi^2}{2\lambda\omega_m\alpha_3} + \frac{2\lambda\omega_m\alpha_3}{\xi}(1+\frac{|\check{E}_x|}{\xi})\right]\delta. \tag{A.16}$$

The bound of $\mathbf{s}^{\mathrm{T}}\mathbf{B}(\mathbf{d}-\check{\hat{\mathbf{d}}})$: The term $\mathbf{s}^{\mathrm{T}}\mathbf{B}(\mathbf{d}-\check{\hat{\mathbf{d}}})$ can be rewritten as:

$$\begin{aligned}\mathbf{s}^{\mathrm{T}}\mathbf{B}(\mathbf{d}-\check{\hat{\mathbf{d}}}) &= \mathbf{s}^{\mathrm{T}}(-\mathbf{I}+\mathbf{B}_2)(\mathbf{d}-\check{\hat{\mathbf{d}}} \pm \hat{\mathbf{d}}) \\ &= -\mathbf{s}^{\mathrm{T}}(\tilde{\mathbf{d}}+\hat{\mathbf{d}}-\check{\hat{\mathbf{d}}}) + \mathbf{s}^{\mathrm{T}}\mathbf{B}_2(\tilde{\mathbf{d}}+\hat{\mathbf{d}}-\check{\hat{\mathbf{d}}}),\end{aligned}$$

where I is the identity matrix,

$$\mathbf{B}_2(\mathbf{E}) = \begin{bmatrix} 0 & b(E) \\ 0 & 0 \end{bmatrix}.$$

For the term $-\mathbf{s}^{\mathrm{T}}(\tilde{\mathbf{d}} + \hat{\mathbf{d}} - \check{\mathbf{d}})$, we derive:

$$-\mathbf{s}^{\mathrm{T}}(\tilde{\mathbf{d}} + \hat{\mathbf{d}} - \check{\mathbf{d}}) \leq |s_1|(|\tilde{d}_1| + |\hat{d}_1 - \check{d}_1|) + |s_2|(|\tilde{d}_2| + |\hat{d}_2 - \check{d}_2|) \leq |s_1|(\gamma_1 + \delta) + |s_2|(\gamma_2 + \delta),$$

where $\gamma_i > |\tilde{d}_i|, i = 1, 2$.

For the term $\mathbf{s}^{\mathrm{T}}\mathbf{B}_2(\tilde{\mathbf{d}} + \hat{\mathbf{d}} - \check{\mathbf{d}})$, we obtain:

$$\mathbf{s}^{\mathrm{T}}\mathbf{B}_2(\tilde{\mathbf{d}} + \hat{\mathbf{d}} - \check{\mathbf{d}}) \leq |s_1||b|(|\tilde{d}_2| + |\hat{d}_2 - \check{d}_2|) \leq |s_1||b|(\gamma_2 + \delta). \tag{A.17}$$

According to (3.4) and Assumption 1, b is bounded:

$$|b| \leq |E_y| + \lambda\omega_m|E_x||\Pi(E_y)| \leq y_m + \frac{2\lambda\omega_m\alpha_3 x_m}{\xi}. \tag{A.18}$$

Combining (A.17) and (A.18):

$$\mathbf{s}^{\mathrm{T}}\mathbf{B}_2(\tilde{\mathbf{d}} + \hat{\mathbf{d}} - \check{\mathbf{d}}) \leq |s_1|\left(y_m + \frac{2\lambda\omega_m\alpha_3 x_m}{\xi}\right)(\gamma_2 + \delta). \tag{A.19}$$

Finally, the boundary value is:

$$\begin{aligned} \mathbf{s}^{\mathrm{T}}\mathbf{B}(\mathbf{d} - \check{\mathbf{d}}) &\leq |s_1|(\gamma_1 + \delta) + |s_2|(\gamma_2 + \delta) + |s_1|\left(y_m + \frac{2\lambda\omega_m\alpha_3 x_m}{\xi}\right)(\gamma_2 + \delta) \\ &\leq |s_1|\left[\left(y_m + \frac{2\lambda\omega_m\alpha_3 x_m}{\xi}\right) + 1\right]\delta \\ &+ |s_1|\left(\gamma_1 + \left(y_m + \frac{2\lambda\omega_m\alpha_3 x_m}{\xi}\right)\gamma_2\right) + |s_2|(\gamma_2 + \delta). \end{aligned} \tag{A.20}$$

Based on the above results, we can obtain:

$$\begin{aligned} &|s_1|\Big\{|v_r|\left[|\cos E_\theta - \cos\check{E}_\theta| + |a(E_y)\sin E_\theta - a(\check{E}_y)\sin\check{E}_\theta|\right] \\ &+ |\omega_r||b(E) - b(\check{E})| + \lambda|\dot{\omega}_r||\Psi(E_y) - \Psi(\check{E}_y)|\Big\} - \mathbf{s}^{\mathrm{T}}\bar{\mathbf{B}}\check{\vartheta} + \mathbf{s}^{\mathrm{T}}\mathbf{B}(E)(\mathbf{d} - \check{\mathbf{d}}) \\ &\leq |s_1|\Big\{v_m\left(1 + 2\sqrt{1 + (\frac{2\lambda\omega_m\alpha_3}{\xi^2})^2}\right) + (\omega_m + k_s)\left(\frac{\xi^2}{2\lambda\omega_m\alpha_3} + \frac{2\lambda\omega_m\alpha_3}{\xi}(1 + \frac{|\check{E}_x|}{\xi})\right) \\ &+ \frac{\xi\dot{\omega}_m}{\omega_m} + \gamma_1 + y_m + \frac{2\lambda\omega_m\alpha_3 x_m}{\xi}\Big\}\delta + |s_1|\left[\gamma_1 + \left(y_m + \frac{2\lambda\omega_m\alpha_3 x_m}{\xi}\right)\gamma_2\right] \\ &+ |s_2|(\gamma_2 + \delta) + k_s\|\mathbf{s}\|. \end{aligned} \tag{A.21}$$

All proofs have been completed here.